Supporting Information

Improved Performance through Tight Coupling of Redox Cycles of Sulfur and 2,6-Polyanthraquinone in Lithium-Sulfur Batteries

Ka-Cheong Lau,[a,b] Ilya A. Shkrob,[a,b] Nancy L. Dietz-Rago,[b] Justin G. Connell,[a] Daniel P. Phelan,[c] Bin Hu,[b] Lu Zhang,[a,b] Zhengcheng Zhang,[a,b] Chen Liao[a,b*]

[a]*Joint Center for Energy Storage Research, Lemont, Illinois 60439, United States*

[b]*Chemical Sciences and Engineering Division, Argonne National Laboratory, Lemont, Illinois 60439, United States*

[c]*Materials Science Division, Argonne National Laboratory, Lemont, Illinois 60439, United States*

*Email: liaoc@anl.gov

S1. Experimental Detail

2,6-Dibromoanthraquinone, bis(pinacolato)diboron, [1,1′-bis(diphenylphosphino)ferrocene]dichloropalladium(II) ((DPPF)$PdCl_2$), K_2CO_3, anhydrous toluene, CH_2Cl_2, $CHCl_3$, CH_3OH, 2,3-dichloro-5,6-dicyano-1,4-benzoquinone (DDQ), THF, sulfur (100 mesh) and anhydrous *N*-methyl-2-pyrrolidone (NMP) were all purchased from Sigma-Aldrich and used as received. CH_3CN and 1,2-dimethoxyethane (DME) were purchased from Sigma-Aldrich and dried over 3 Å molecular sieves. Conductive carbon C45 nanoparticles (60-70 nm) were purchased from Timcal. Lithium bis(trifluoromethane)sulfonamide (LiTFSI) was purchased from Solvionic and dried at 150 °C under vacuum overnight prior to use. Polyvinylidene difluoride (PVdF) was purchased from Solvay. 1,1,2,2-tetrafluoroethyl 2,2,3,3-tetrafluoropropyl ether (TTE) was purchased from SynQuest and dried over 3 Å molecular sieves overnight.

Synthesis of 2,6-Polyanthraquinone (PAQ). PAQ was synthesized following the modified literature procedures.[1,2] 2,6-Dibromoanthraquinone (10.0 g, 27.3 mmol), bis(pinacolato)diboron (7.01 g, 27.6 mmol), (DPPF)$PdCl_2$ (1.17 g, 1.60 mmol), toluene (1 L), and a solution of K_2CO_3 in deionized water (0.5 M, 200 mL, 100 mmol) were placed in a Schlenk flask. The suspension was sparged with N_2 for 30 min at room temperature, and then stirred at 130 °C in a sand bath under N_2. After three days, the mixture was cooled down to room temperature and poured into

CH_2Cl_2 (500 mL) under ambient pressure. The precipitate was filtered out and washed sequentially with water, CH_3OH, $CHCl_3$, and toluene. The solid was suspended in THF (15 mL), and DDQ (7.95 g, 35.0 mmol) was then added to this mixture. The reaction mixture was stirred at room temperature for 12 h. The solution was filtered, and a dark brown solid material was collected on the filter. This material was washed with THF and dried under vacuum at 100 °C for 10 h to yield a brown powder (7.49 g). The infrared (IR) spectrum of this powder closely resembles the IR spectrum of PAQ in literature (see Figure S1).[1,2] In Table S1, the vibration frequencies of PAQ are compared with those observed from various anthraquinone derivatives. Interestingly, one of the minor bands in Figure S1 coincides with the C=C stretch in 2-bromoquinone, and we surmise that this feature may originate from a small fraction of the brominated chain termini (as is also suggested by the X-ray photoelectron spectra shown below).

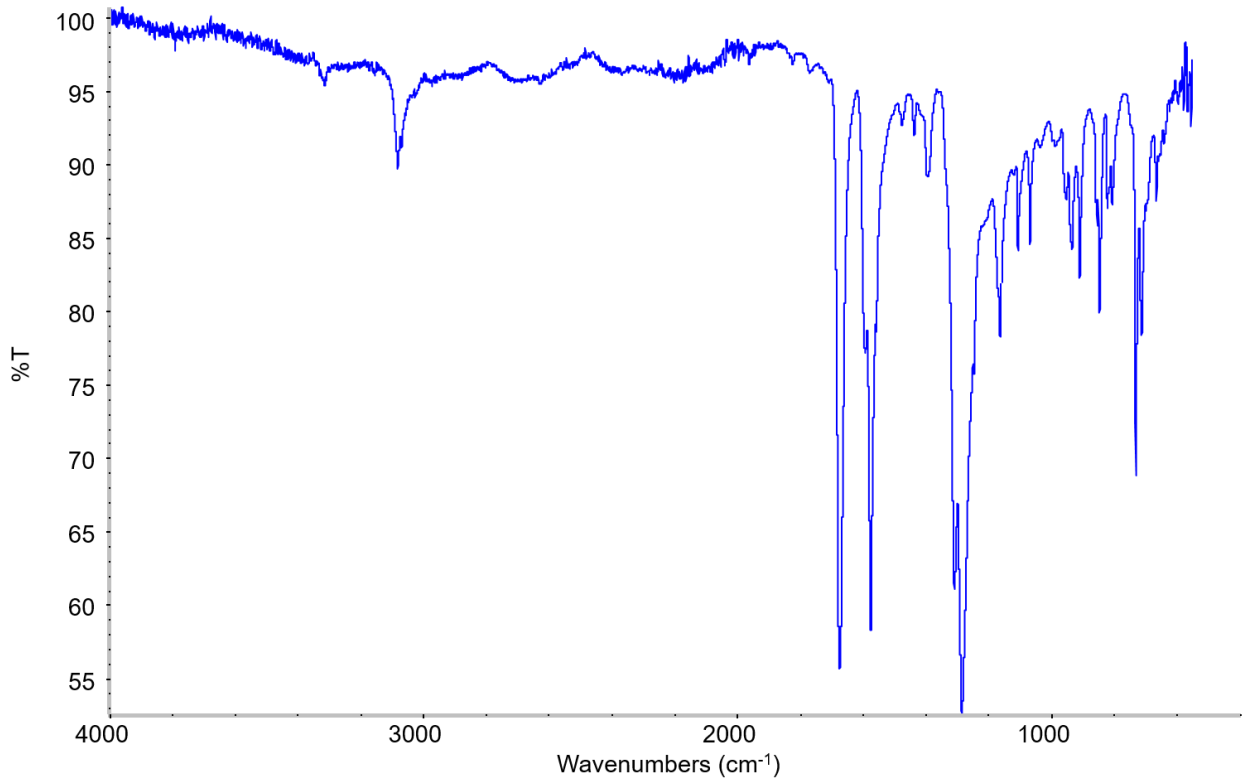

Figure S1.The infrared transmission spectrum of PAQ.

Table S1. Vibration frequencies for C−H, C=O and C=C bonds in anthraquinone, 2-bromoanthraquinone, 2,6-dibromoanthraquinone, and PAQ.

ν (cm^{-1})	C−H	C=O	C=C
Anthraquinone[3]	3074	1680	1592
2-Bromoanthraquninone[4]	3079	1678	1578
2,6-Dibromoanthraquinone[5]	3093	1685	1582
PAQ	3072	1675	1592, 1578

This powder was also analyzed using X-ray photoelectron spectroscopy (XPS). The survey spectrum shown in Figure S2 indicates a C:O atomic ratio of 7:1, which is consistent with the $C_{14}O_2H_x$ backbone of PAQ; trace amount of Br atoms from the polymer chain termini were also observed. Pd 3d core level spectrum indicates the presence of trace amount of Pd atoms (< 0.1 at%) which were not observed in the starting AQ material (Figure S3).

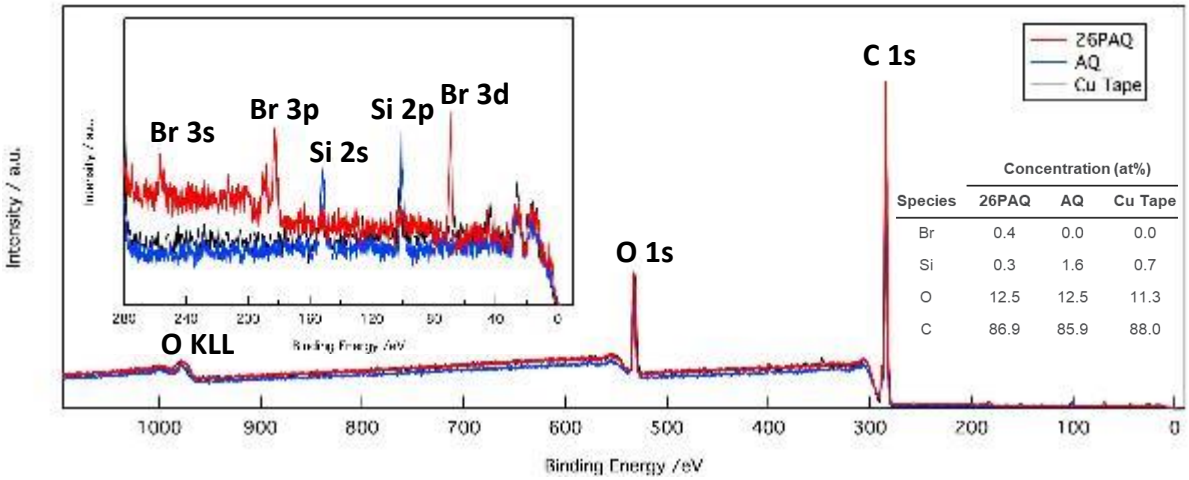

Concentration (at%)

Species	26PAQ	AQ	Cu Tape
Br	0.4	0.0	0.0
Si	0.3	1.6	0.7
O	12.5	12.5	11.3
C	86.9	85.9	88.0

Figure S2. Survey X-ray photoelectron spectrum of PAQ *(red)* and solid anthraquinone (AQ, *blue*).

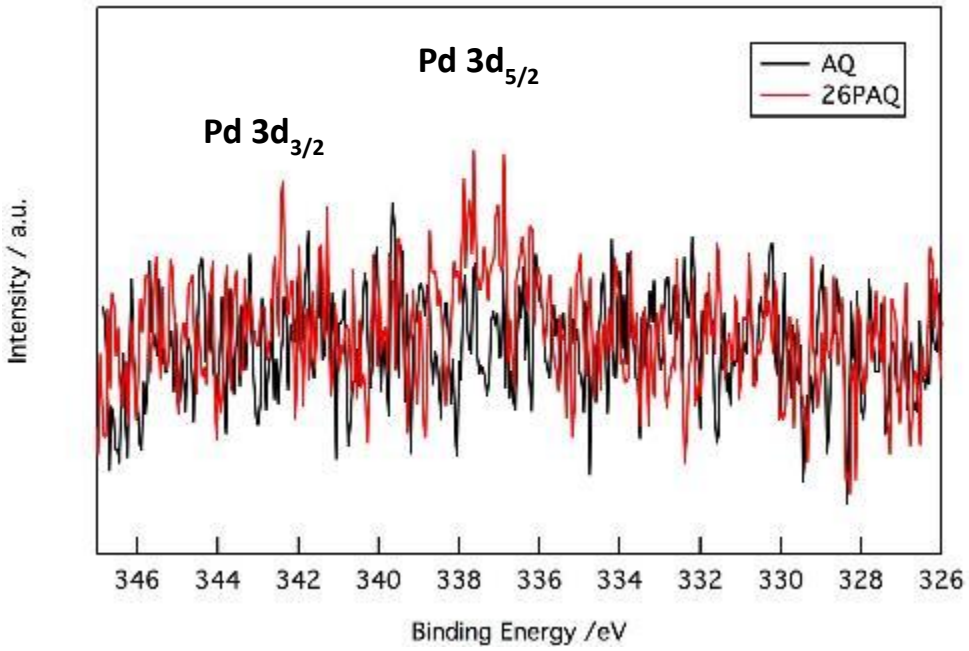

Figure S3. XPS Pd 3d spectrum of PAQ and anthraquinone (AQ).

Synthesis of Lithium 2,6-Polyanthraquinonide (Li[PAQ]). Under Ar, freshly cut lithium (3.7 mg, 0.53 mmol) and naphthalene (78 mg, 0.61 mmol) were placed in a glass vial. As THF (2 mL) was added, the mixture turned dark green in 5 s. The mixture was stirred at room temperature for 5 min to yield a homogeneous dark green solution. PAQ (112.5 mg, nominally 0.55 mmol AQ units) was added to this solution, and the mixture was stirred for additional 15 min to give a dark brown slurry. The brown supernatant was decanted, and the residue was washed with *n*-pentane (5 mL × 3) to give Li[PAQ] as a dark brown powder (102 mg, 0.48 mmol AQ units, 91 % yield).

Synthesis of Dilithium 2,6-Polyanthraquinonide (Li_2[PAQ]). Under Ar, freshly cut lithium (6.1 mg, 0.88 mmol) and naphthalene (120 mg, 0.94 mmol) were placed in a vial. THF (2 mL) was added, and the mixture turned dark green in 5 s. The mixture was stirred at room temperature for 3 min to yield a homogeneous dark green solution. PAQ (92.1 mg, nominally 0.45 mmol AQ units) was added to this solution, and the mixture was stirred for 15 min to give a brown-red slurry. The red supernatant was decanted, and the residue was washed with *n*-pentane (5 mL × 3) to give Li_2[PAQ] as a red powder (93 mg, 0.42 mmol AQ units, 95 % yield). Li_2[PAQ] was suspended in THF, filtered and analyzed using gel permeation – size exclusion chromatography. The elution of Li_2[PAQ] in THF was carried out at 1 mL/min and 30 °C using an Agilent 1260 Infinity II chromatograph with a refractive index detector. A PLgel 5 μm guard column and three PLgel 5 μm mixed-B columns (all from Agilent) were used in combination. Narrow-dispersed polystyrene standards (Agilent EasiVial PS-M) were used for calibrations, and the data were processed using Cirrus GPC/SEC software. The number average molecular weight (M_n) of Li_2[PAQ] was ~71 kDa and the polydispersity index (M_w/M_n, which is the ratio of the mass and the number average molecular weight) was ~2.14.

Synthesis of Lithium Tetrasulfide (Li_2S_4).[6] Under N_2, S_8 (513.8 mg, 2.0 mmol) and THF (10 mL) were placed in a Schlenk flask to form a yellow suspension. A solution of $LiEt_3BH$ in toluene (1 M, 8 mL, 8 mmol) was added dropwise to this suspension and it gradually turned to a homogeneous orange solution with the concomitant gas evolution. Volatiles were removed under vacuum to afford nominally Li_2S_4 compound as an orange-yellow powder.

Reactions of PAQ Derivatives with Sulfur Species. Under Ar, a PAQ polymer (PAQ, Li[PAQ] or Li_2[PAQ]; 20 mg) was placed in a glass vial. A solution of Li_2S_4 in DME (nominally 50 mM, 2 mL, 0.10 mmol), a suspension of Li_2S in DME (nominally 65 mM, 2 mL, 0.13 mmol), a suspension of Li_2S_4 in $(CH_3CN)_2$LiTFSI/TTE (50 mM, 2 mL, 0.10 mmol) or a suspension of Li_2S in $(CH_3CN)_2$LiTFSI/TTE (50 mM, 2 mL, 0.10 mmol) was added, and the mixture was stirred at 55 °C for 24 h. Volatiles were removed under vacuum, and the resulting solid residue was analyzed using infrared spectroscopy.

S2. Magnetometry for Li[PAQ] polymer

The magnetometry of Li[PAQ] was carried out using a Quantum Design Magnetic Property Measurement System 3 by warming the sample from 2 K to 300 K in a flow of helium in 1 kOe. Let $\chi = dM/dH$ be the magnetic susceptibility, M be the magnetic moment, H be the magnetic field outside of the sample, N be the number of spin-1/2 centers, $\beta = 1/k_B T$, T be the temperature, and k_B be the Boltzmann constant. For an isolated S = 1/2 radical, the effective magnetic moment $\mu_{eff}^0 / \mu_B = g\sqrt{S(S+1)} \approx 1.73$, where μ_B is the Bohr magneton and g is the g-factor determined from our EPR measurements (see section S4 below). In the low-field, high-temperature limit, the magnetization χ of a paramagnetic sample in the vanishing magnetic field follows the Curie-Weiss law

$$\chi_{H\to 0} = \frac{N\left(\mu_{eff}^0\right)^2}{3k_B(T-\Theta)} \qquad \text{(eq. S1)}$$

where Θ is the Curie-Weiss temperature, so that χ^{-1} is a linear function of the temperature. In the general case, the effective magnetic moment μ_{eff} is defined from

$$\chi_{H\to 0} = \frac{N\beta\mu_{eff}^2}{3} \qquad \text{(eq. S2)}$$

For an infinite antiferromagnetic (AF) alternating linear chain of spin-1/2 centers $\hat{S}_i$ interacting as

$$H_{ex} = -2J_{ex}\sum_{i=1}\left[\hat{S}_{2i} \bullet \hat{S}_{2i-1} + \alpha\,\hat{S}_{2i} \bullet \hat{S}_{2i+1}\right] \qquad \text{(eq. S3)}$$

via isotropic Heisenberg exchange between the neighboring spins ($0 \le \alpha \le 1$, $J_{ex} < 0$), there is the well-known Hatfield's approximate formula

$$\left(\frac{\mu_{eff}}{\mu_{eff}^0}\right)^2 \approx \frac{1 + Ax + Bx^2}{1 + Cx + Dx^2 + Fx^3} \qquad \text{(eq. S4)}$$

where $x = 1/\beta|J_{ex}|$ and the coefficients A to F are polynomial functions of α. The explicit expressions for these coefficients are given in ref. 7.

In Figure S4, panel a shows the linear fit of the high-temperature (50 – 300 K) section of the χ^{-1} vs. T plot to the Curie-Weiss law (given by eq. S2) for Li[PAQ], which corresponds to $\mu_{eff}^0 / \mu_B \approx 1.673 \pm 0.001$ per unit equivalent and $\Theta \approx -36.55 \pm 0.14$ K. In this estimate, we took into account that our polymer sample contained residual solvent (section S9 below); also, the magnetic susceptibility χ was corrected by the temperature-independent diamagnetic contribution $\chi_0 \approx -1.2 \times 10^{-4}$ emu/mol as determined form the least-squares fit. The extrapolated

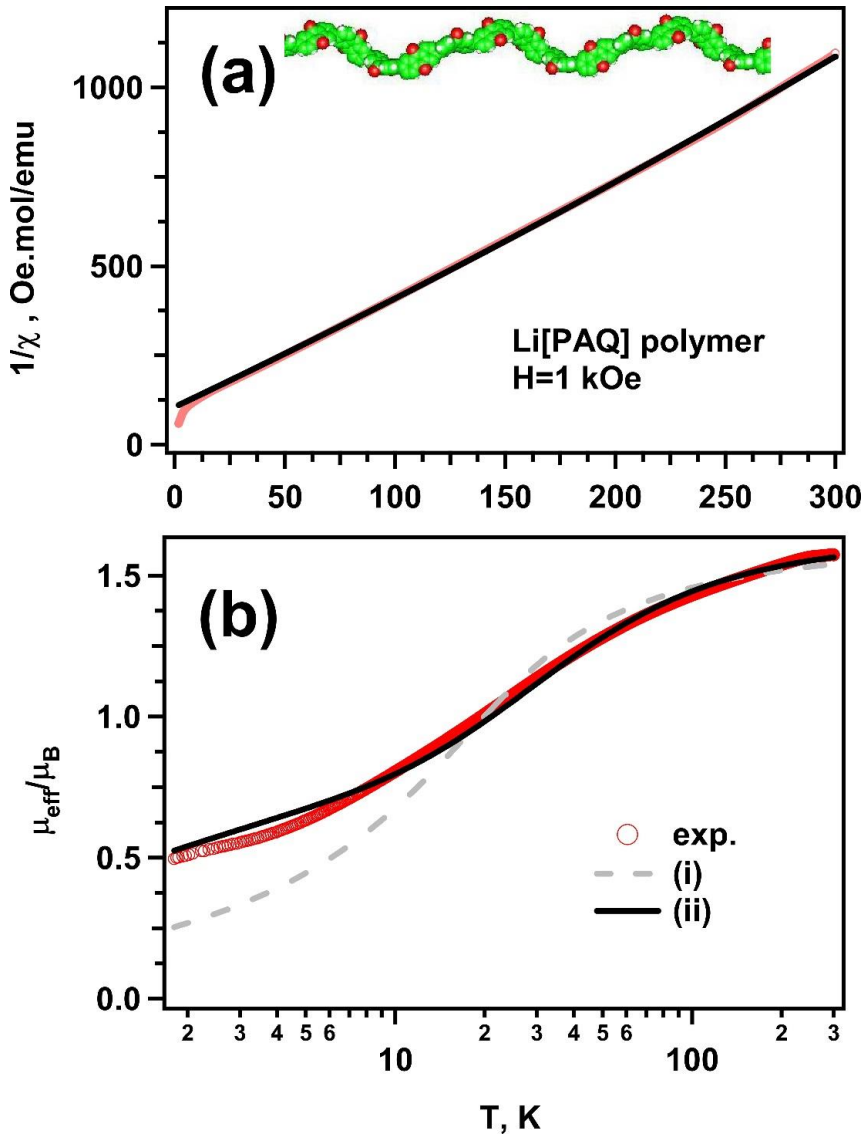

Figure S4. (a) Reciprocal molar magnetic susceptibility χ^{-1} vs. temperature for dry, solid Li[PAQ] polymer (*red open circles*). The solid line is the best Curie-Weiss fit in the 50 – 300 K region. Shown at the top is the space filling model for the helical Li[PAQ] polymer (the lithium ions have been removed for clarity) with the green, white and red balls indicating C, H, and O atoms, respectively. The helicity of the chain originates through the nearly 90° angle between the arene rings belonging to the neighboring $Li^{+}AQ^{-\bullet}$ units. (b) The fit of μ_{eff} (*red open circles*) to the Hatfield's formula for the linear, alternating, antiferromagnetically ordered spin-1/2 chain. Trace ii is for $\alpha = 1$ (no alternation) and trace i is for $\alpha < 1$ (alternation). The optimized model parameters are given in the text above.

μ_{eff}^{0} / μ_{B} is within 4 % of the theoretical value of 1.74, suggesting that almost every functional unit in the Li[PAQ] polymer bears an unpaired localized electron. The negative Curie-Weiss temperature also suggests AF ordering between these neighboring spins. In Figure S4, panel b

we fit the low-temperature μ_{eff} to eq. S4. For $\alpha = 1$ (non-alternating spin-1/2 chain), the fit quality was poor (see trace ii in Figure S4, panel b). The best fit was obtained for $\mu_{eff}^{0} / \mu_B \approx$ 1.625 ± 0.0005, $\alpha \approx 0.723 \pm 0.001$, and $2J_{ex} \approx$ -53.6 ± 0.2 K (which is equivalent to -37.3 cm^{-1}; see trace i in Figure S4, panel b). Thus, in the Li[PAQ] polymer there is AF coupling between the neighboring spins on the chain that can be neglected only in the high temperature limit ($x << 1$), at which our EPR spectra were obtained. The alternation of the spin exchange constants strongly suggests a helical conformation of the polymer chains that is also suggested by our molecular modeling (see the inset in Figure S4, panel a).

S3. Additional cycling data for S_{cath} and S-PAQ_{cath} cells

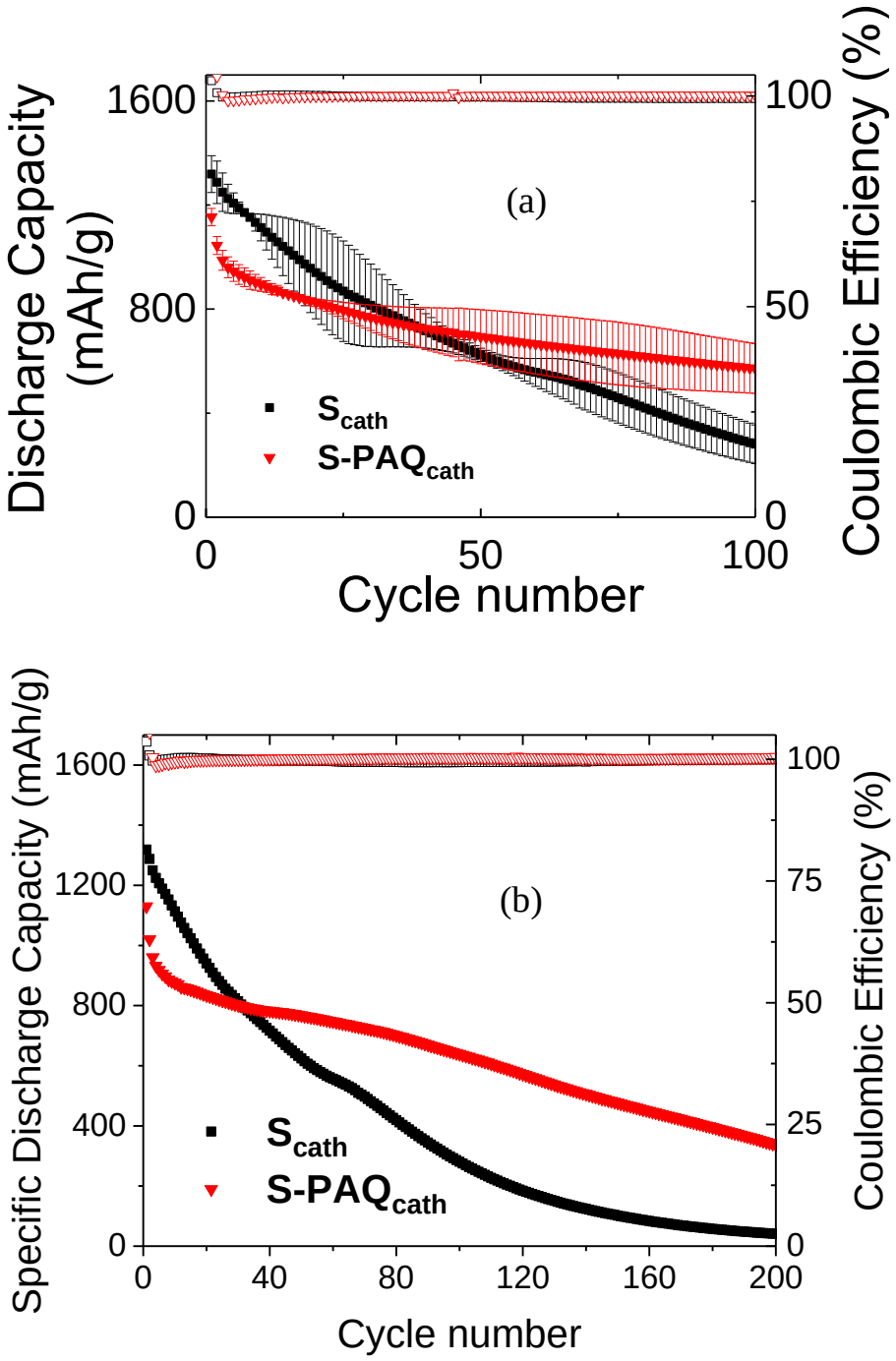

Figures S5a,b. The specific discharge capacity (*left axis, filled symbols*) and coulombic efficiency (*right axis, open symbols*) plotted vs the number of cycles for **S_{cath}** (*black*) and **S-PAQ_{cath}** (*red*) cells cycled at C/10 rate and 55 °C. In panel a, the standard deviations for Figure 1c are shown. In panel b, extended cycling data are shown.

S4. Electron paramagnetic resonance (EPR) experiments

Continuous-wave Electron Paramagnetic Resonance (EPR) spectroscopy was used to characterize the reduced PAQ polymers suspended in liquid solutions at 300 K. To this end, 100 μL aliquots were placed in the borosilicate glass capillaries and these capillaries were then sealed in glass tubes to prevent contact with air. The first-derivative EPR spectra were obtained using a Bruker ESP300E X-band spectrometer operating at 9.4383 GHz, 2 mW, and 0.2 G field modulation at 100 kHz. The hyperfine structure in these EPR spectra was analyzed using a WinSim program suite.

First, we consider the EPR spectrum of Li[PAQ] polymer in THF that is shown in Figure S6, panel a. In this experiment, PAQ suspended in THF was reduced using 1 equivalent of lithium h_8-naphthalenide as described in section S1. The extracted Li[PAQ] polymer was dried under argon to the constant weight and used in the subsequent experiments. In the control experiments, we synthesized this Li[PAQ] polymer using perdeuterated naphthalene; no difference in the properties between the two materials was found. Importantly, our magnetic measurements of the Li[PAQ] polymer (section S2) indicate that in this polymer nearly every unit contained an unpaired electron, i.e. the EPR signal originated from the spin centers in the polymer chains as opposed to a paramagnetic impurity. These magnetic measurements also suggested that 300 K corresponds to the high-temperature limit in which the spin exchange coupling between the neighboring spins on the polymer chain can be neglected.

Figure S6 shows the EPR spectrum of the Li[PAQ] polymer suspended in THF; for comparison, EPR resonances from the naphthalenide radical anions ($Np^{-\bullet}$) in THF with g = 2.0038 are shown (note that H/D substitution in these anions causes the "collapse" of the resonance line since the hyperfine coupling constants for the deuterons are only ~15% of the proton ones). It is seen that unreacted $Np^{-\bullet}$ has been completely removed. The residual EPR signal is a multiplet of resonance lines with g = 2.0061. This g-factor is considerably higher than 2.0043 – 2.0045 for isolated anthraquinone semiquinone radicals, $AQ^{-\bullet}$ and $Li^{+}AQ^{-\bullet}$, in THF, according to the literature (Table S2). Comparisons with the reported proton hyperfine coupling constants (hfcc's) for these two radicals (cf. the simulations in Figure S7 and hfcc parameters in Table S2) suggests that the observed EPR signal originates from non-interacting spin-1/2 centers on the polymer chain, whose hfcc's are fairly close to the ones reported for the free $Li^{+}AQ^{-\bullet}$ radicals and rather different from the free $AQ^{-\bullet}$ radical anions (Table S2). This analysis suggests that in Li[PAQ] suspension in THF (i) the Li^{+} ions are strongly associated with the $AQ^{-\bullet}$ units in the polymer chains, thereby breaking the local central symmetry of the $AQ^{-\bullet}$ units; (ii) as the polymer chains move, these $AQ^{-\bullet}$ radicals rapidly tumble, so there is efficient averaging of anisotropic magnetic interactions, and (iii) these $AQ^{-\bullet}$ radicals weakly interact with each other despite their local high concentration. The relative weakness of these magnetic interactions can be explained by poor conjugation in the $(Li^{+}AQ^{-\bullet})_{\infty}$ chains: the neighboring aromatic moieties are nearly perpendicular to each other, so the spin exchange and magnetic dipole-dipole interactions are greatly reduced.

Figure S8 shows *in situ* generation of the Li[PAQ] polymer: the suspension of PAQ in THF was treated with 1 equivalent of lithium d_8-naphthalenide. *Ca.* 15 min into this reaction, the EPR signal from the naphthalenide entirely disappeared, and the characteristic multiplet of the resonance lines from the Li[PAQ] polymer appeared (compare Figures S6 and S8). The EPR signal in this reaction mixture originates entirely from the suspended polymer particles. Indeed,

passing of the suspension through 0.2 μm pore Teflon filter removed 60 % of the initial EPR signal, and further centrifuging of this filtrate removed 95 % of the initial EPR signal (see Figure S8). Thus, the EPR signal from Li[PAQ] (despite the excellent averaging of magnetic anisotropies) *originates from the polymer particles* as opposed to isolated polymer chains in the solution. All of these observations indicate considerable chain mobility of Li[PAQ] coils in THF.

The situation was clearly different in the $(CH_3CN)_2$LiTFSI/TTE solution (Figure 4 in the text). Suspended Li[PAQ] in this solvent (Figure 4b) yielded a poorly resolved singlet at g = 2.0057, indicating insufficient averaging of magnetic anisotropies in the $Li^+AQ^{-\bullet}$ units. Nearly the same EPR signal was observed when PAQ was reacted *in situ* with Li_2S_4 in this solvent (Figure 4), i.e. this reaction generates a polymer with the similar properties to Li[PAQ] polymer obtained by chemical reduction of PAQ in THF using the lithium naphthalenide. Very similar EPR signal (albeit a weaker one) was observed when Li[PAQ] polymer was suspended in CH_3CN/TTE mixture with and without LiTFSI (Figure 4). The same broad EPR singlet was observed in neat TTE (Figure S9a), whereas the EPR signal in neat CH_3CN was much narrower (Figure S9a): the peak-to-peak distance decreased from 7.4 G in TTE to 2.8 G in CH_3CN. While the EPR line in CH_3CN is not resolved (as opposed to THF), the second moment M_2 of this resonance line (1.93 G^2) is very close to that of Li[PAQ] in THF, $M_2 \approx 1.87$ G^2 (Figure S6), suggesting that this resonance line originates from the same $Li^+AQ^-\bullet$ radicals, albeit inhomogeneously broadened due to their slower tumbling. It appears, therefore, that the transformation of the EPR spectrum into the broad Lorentzian line is caused *specifically by the TTE component in the solution.* Once TTE replaces THF molecules solvating the Li^+ ions, the polymer undergoes a dramatic transformation.

Our EPR experiments indicate that this transformation is not only dramatic, but also irreversible. When the Li[PAQ] polymer synthesized in THF is exposed to the $(CH_3CN)_2$LiTFSI/TTE solution and then re-suspended in THF (Figure S9b), the EPR spectrum shows a broad component in addition to the well-resolved multiplet of Li[PAQ] as observed in THF. This broad component is observed even after 12 h of stirring the solution at 60 °C, suggesting that the solvent molecules cannot reach into the particle core. The same applies to the polymer synthesized in the reaction of PAQ with Li_2S_4 in the $(CH_3CN)_2$LiTFSI/TTE solution (Figure S9b) that was suspended in THF. Only a broad EPR signal was observed, and the characteristic multiplet from the Li[PAQ] in THF did not recover even after 2 – 12 h stirring of this THF solution at 60 °C.

The broadening of the EPR spectrum indicates poor averaging of magnetic anisotropies caused by the inhibited chain motions in the polymer coil. The latter can be expected if the polymer coil undergoes a hydrophobic collapse as the THF molecules (that complete the solvation shell of Li^+ ions) are replaced by TTE molecules. Once the coil collapses, the trapped Li^+ ions become shared by several functional units, and the polymer effectively becomes cross-linked. Consequently, the exposure of the collapsed polymer coil to THF does not cause the uncoiling of the polymer chains as the THF molecules cannot diffuse into the core to solvate Li^+ ions.

Thus, the Li[PAQ] polymer in the TTE-containing solvate is structurally similar, but morphologically different from the same polymer in THF and acetonitrile. It is not presently clear whether these differences affect the electrochemical performance of PAQ in the TTE-containing solvate electrolytes.

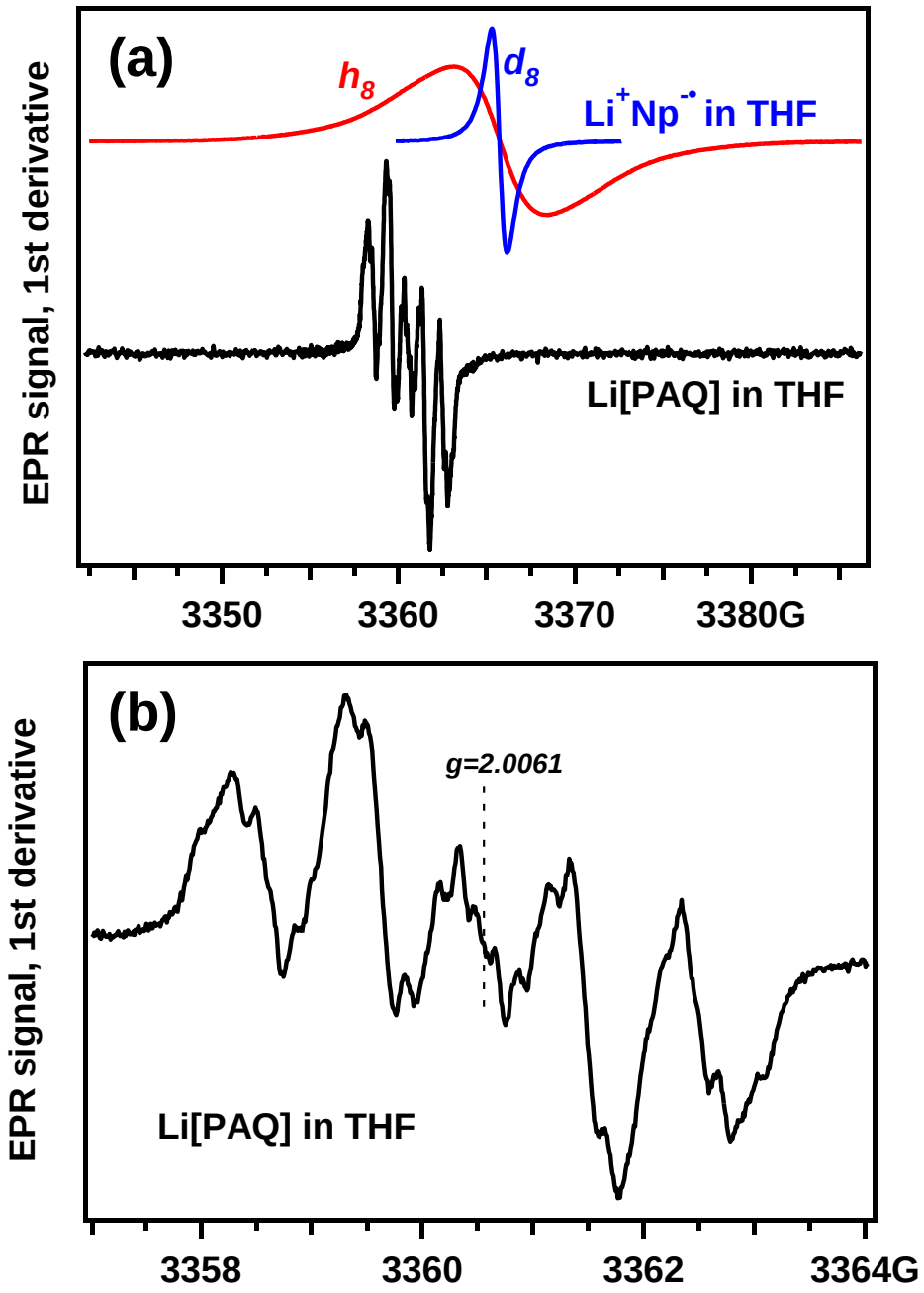

Figure S6. First-derivative X-band continuous wave EPR spectra of (a) lithium h_8- or d_8-naphthalenide in THF at 25 °C (g = 2.0038 signals shown at the top) and the multiplet of resonance lines indicating well resolved hyperfine structure from the suspended Li[PAQ] polymer in the same solvent (g = 2.0061 signal shown to the bottom). The central section of this EPR spectrum is shown separately in panel b.

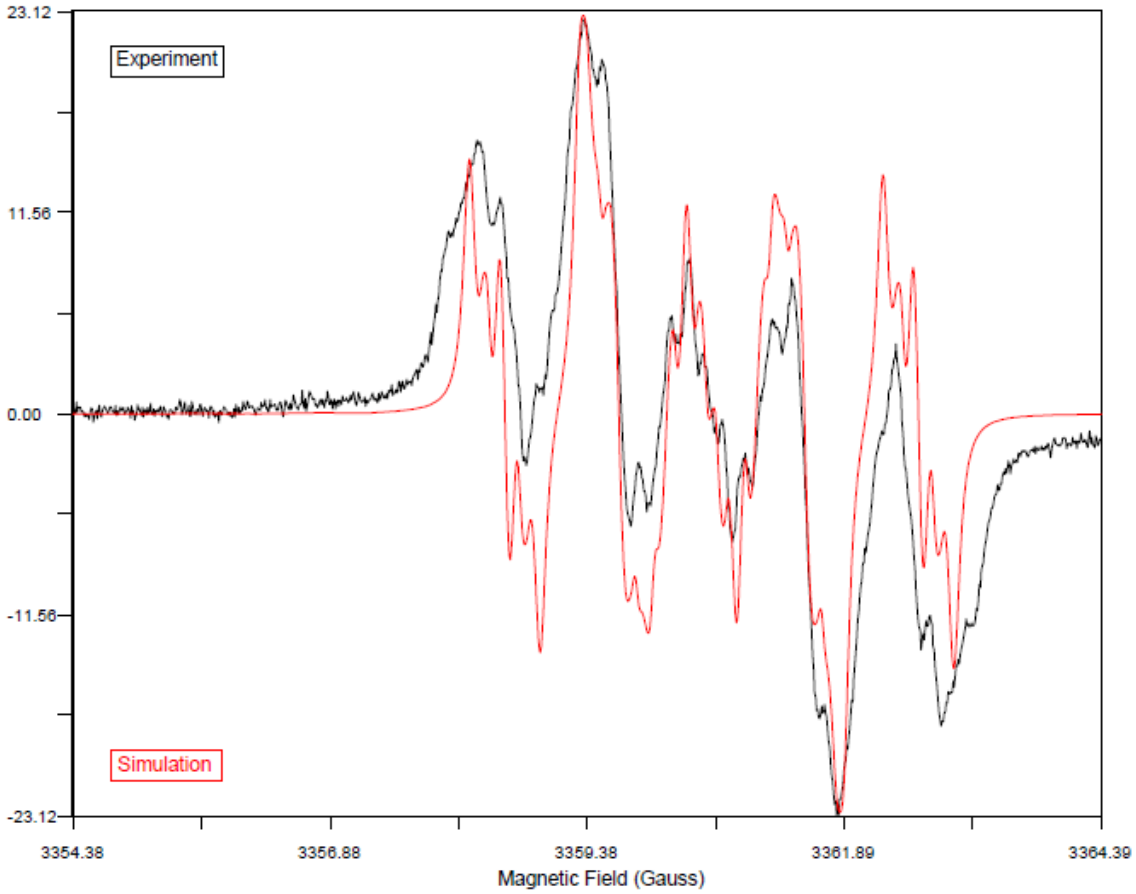

Figure S7. Experimental first-derivative EPR spectrum of Li[PAQ] in THF at 25 °C reproduced from Figure S7, panel b (*black line*) compared to the simulated EPR spectrum of an isolated $Li^{+}(C_{14}H_6O_2^{-\bullet})$ unit obtained using the magnetic parameters given in Table S2 (*red line*).

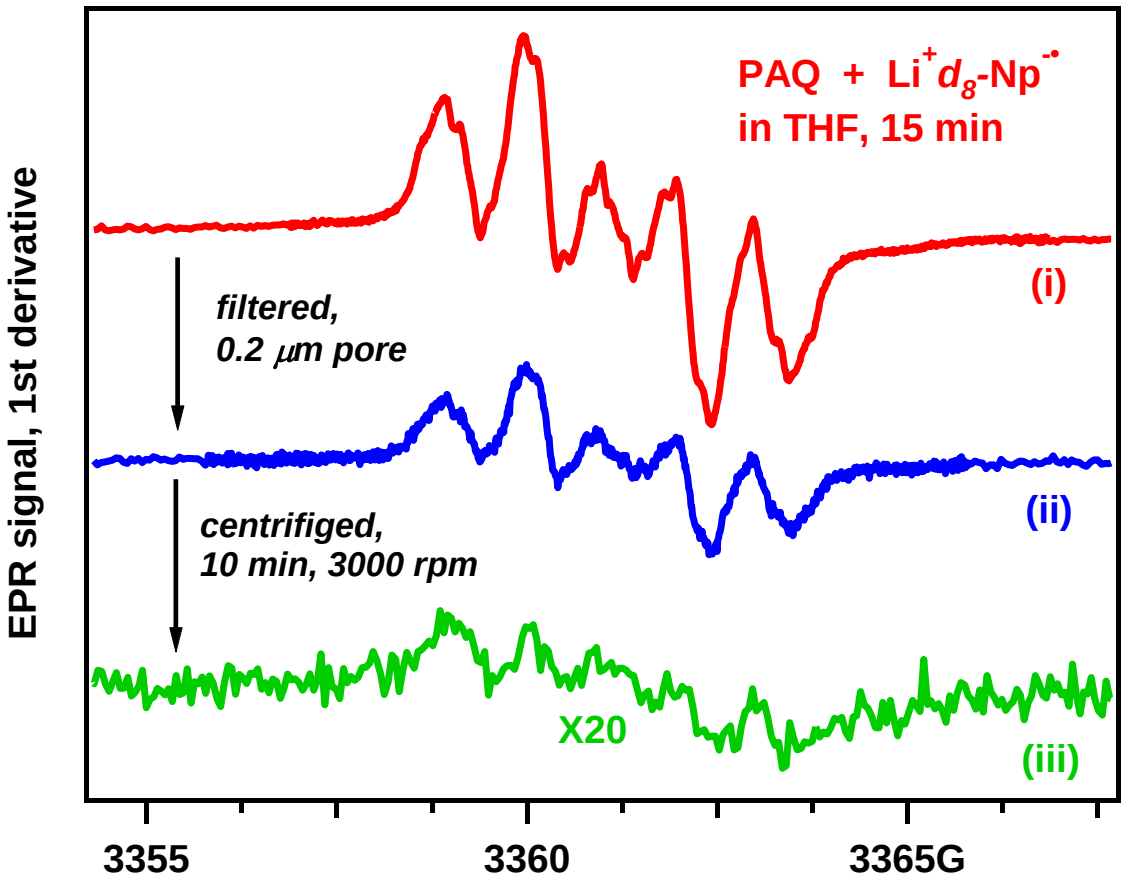

Figure S8. *In situ* formation of Li[PAQ] in THF. First-derivative X-band continuous wave EPR spectra of (i) equimolar mixture of PAQ and lithium d_8-napthalenide obtained 15 min after the initiation of the PAQ reduction. By this time, the EPR signal of $Li^+Np^{-\bullet}$ (a narrow singlet at g = 2.0038) disappeared (Figure S7, panel a) and the EPR signal of Li[PAQ] at g = 2.0061 appeared. (ii) Passing of this reaction mixture through a 0.2 μm pore Teflon filter removed 60 % of the observed EPR signal while (iii) further centrifuging this filtrate for 10 min at 3,000 rpm removed almost all of the observed EPR signal (mind the amplification factor of X20 for trace iii). This experiment proves that the EPR signal originates entirely from the polymer particles/globules suspended in the THF solvent.

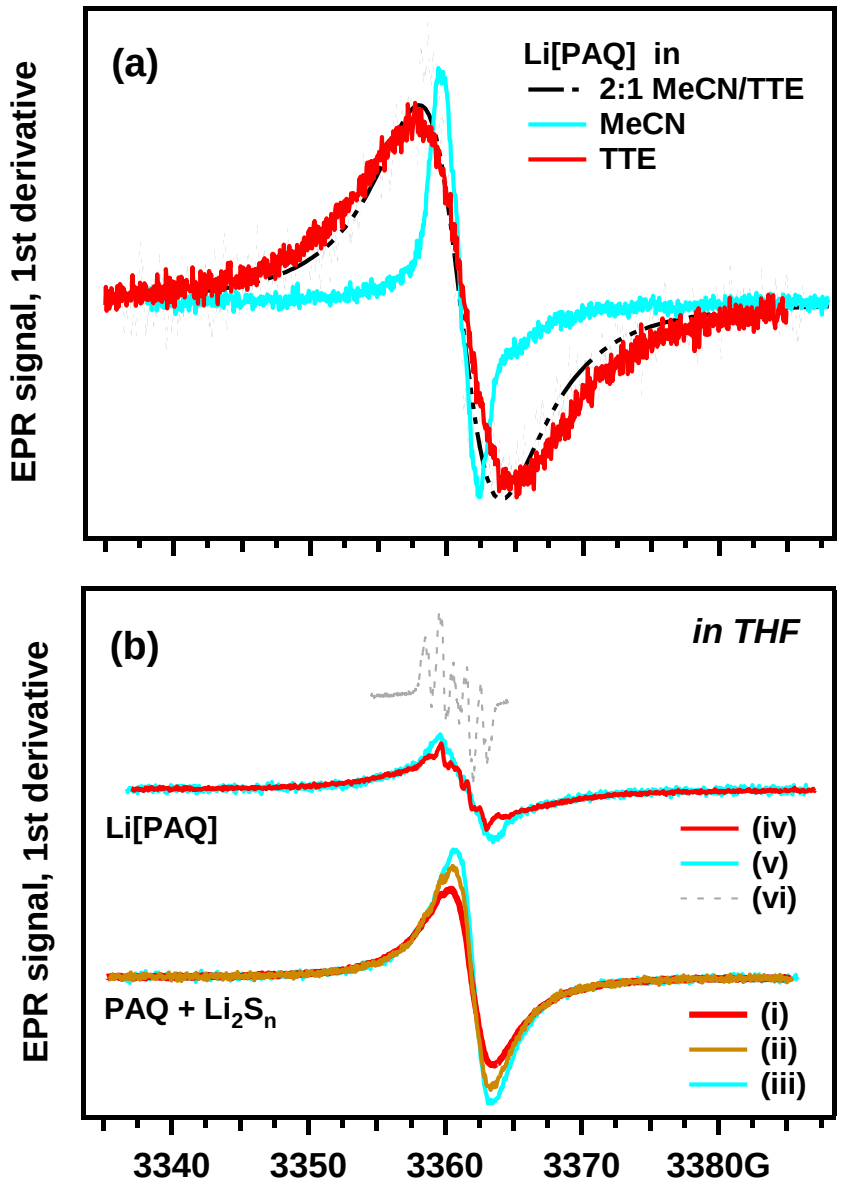

Figure S9. (a) First-derivative EPR spectra of the Li[PAQ] polymer (originally synthesized in THF) suspended in 1:1 v/v CH_3CN/TTE mixture and in neat MeCN and TTE separately. It is seen that the strong broadening of the EPR line is observed only in the TTE-containing solutions. (b) EPR spectra of the polymers in THF. Traces i-iii are for the polymer that was synthesized by reacting equimolar mixture of PAQ and Li_2S_n in the solvate (nominally, n=4). Traces iv and v are from Li[PAQ] polymer that was synthesized in THF, suspended in the solvate, and then removed from the solvate and suspended in THF. For comparison, the EPR spectrum of Li[PAQ] in THF is given in trace vi. Traces i and iv were obtained shortly after suspending these polymers in THF, and traces iii and iv were obtained after stirring these THF solutions for 12 h at 60 °C. Trace ii was obtained after 2 h stirring. All EPR spectra were obtained at 25 °C.

Table S2. Magnetic parameters for anthraquinone ($AQ^{-\bullet}$) radicals in THF (25 °C).

Radical anions	***g*-2, x10^4**	**hfcc's (Gauss)** [c]			
		1,8	**2,7**	**3,6**	**4,5**
$AQ^{-\bullet}$ [a]	45.5	0.244	0.998	0.998	0.244
Li^+ $AQ^{-\bullet}$ [a]	43.1	1.093	0.17	1.804	0.309
Li[PAQ] [b]	61.0	1.071 1.142	0.109	1.811	0.186 0.293

The protons are numbered as shown in the scheme below. a) taken from ref. 8; b) this study (see Figure S7 for simulation); c) isotropic hyperfine coupling constants (hfcc's) for ^{1}H nuclei.

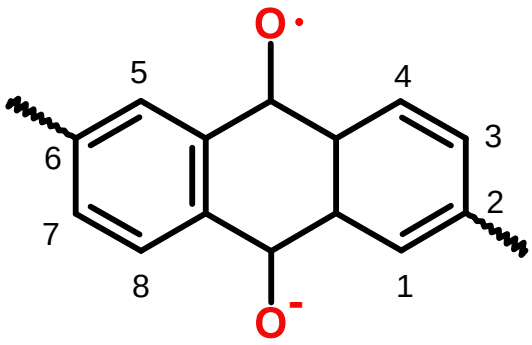

S5. Infrared absorption spectra of the polymers

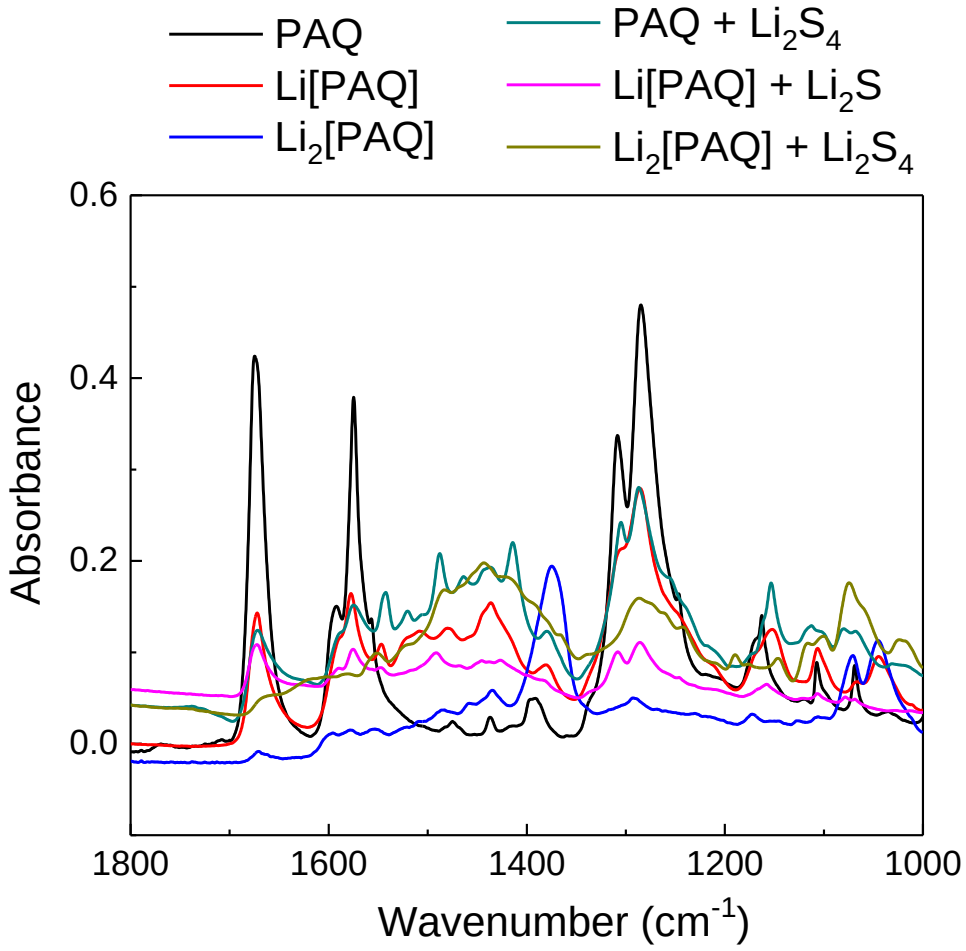

Figure S10a. Infrared absorption spectra of PAQ, Li[PAQ], and Li_2[PAQ] polymers and the solid products of their reactions with Li_2S_4 and Li_2S in DME. The color coding of the traces is given in the legend placed to the top.

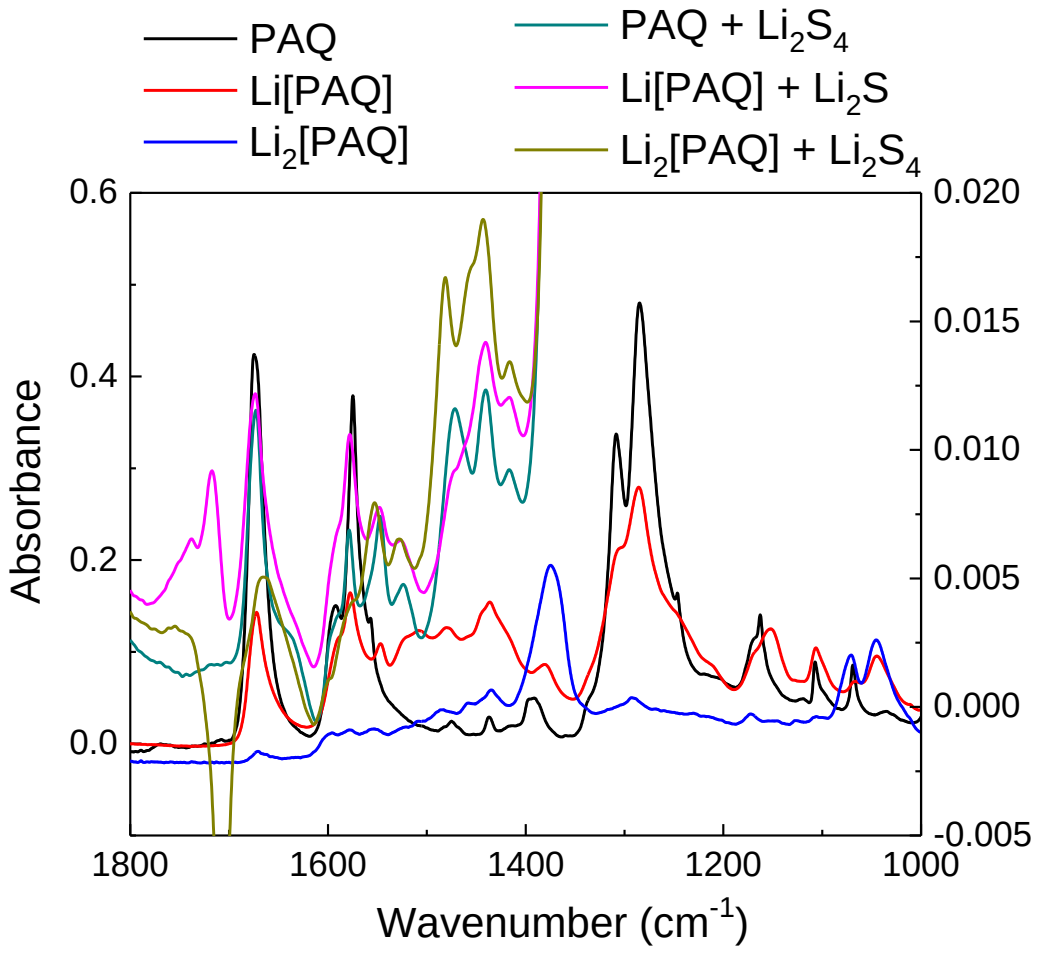

Figure S10b. Infrared absorption spectra of PAQ, Li[PAQ], Li_2[PAQ] polymers and the products of their reaction with Li_2S_4 and Li_2S in $(CH_3CN)_2$LiTFSI/TTE. The vibration bands with the wavenumber between 1000 cm^{-1} and 1400 cm^{-1} belong to LiTFSI. *Left axis:* PAQ, Li[PAQ], Li_2[PAQ]. *Right axis:* the products of reactions with Li_2S_4 or Li_2S. The color coding of the traces is given in the legend to the top.

S6. Supplementary SEM images and EDS analyses

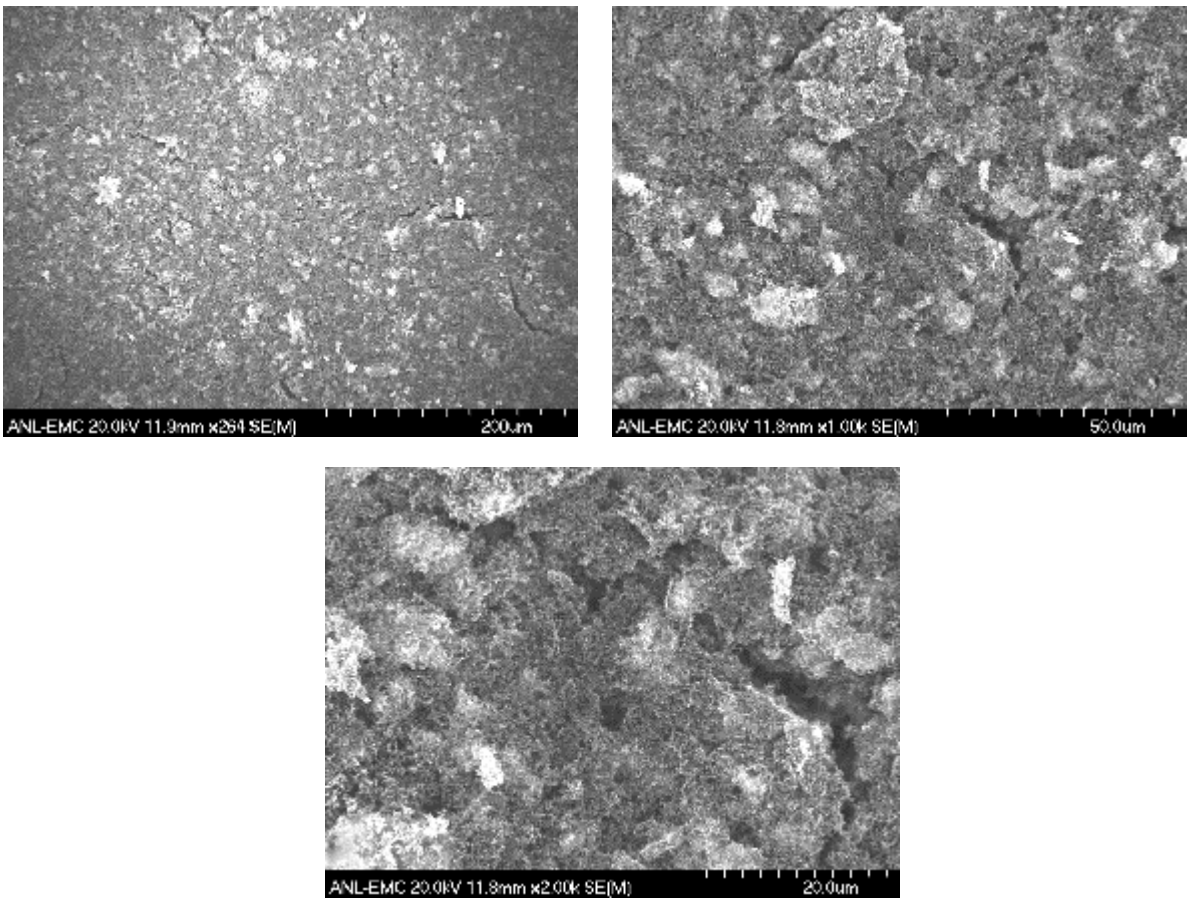

Figure S11. SEM images of the pristine $\mathbf{S_{cath}}$ cathode.

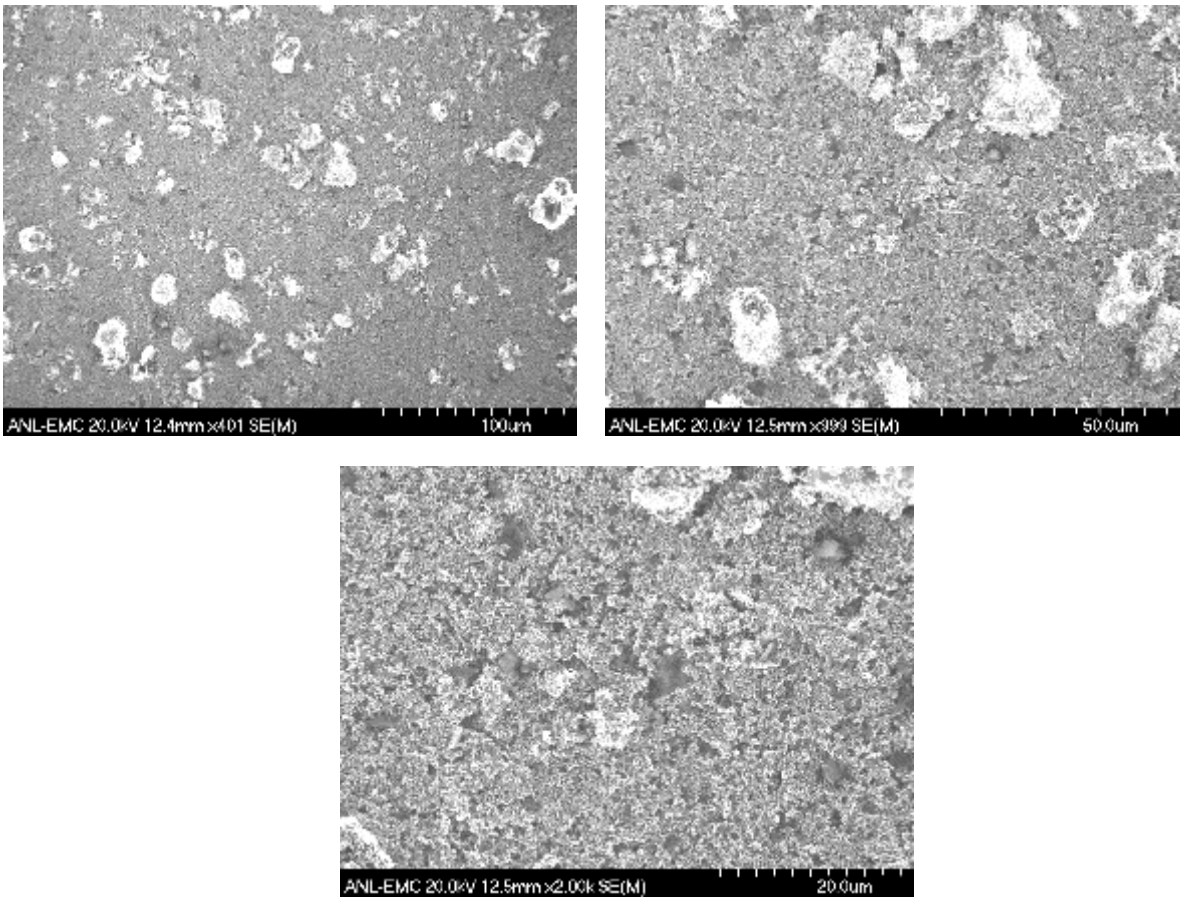

Figure S12. SEM images of the pristine **S-PAQ$_{cath}$** cathode.

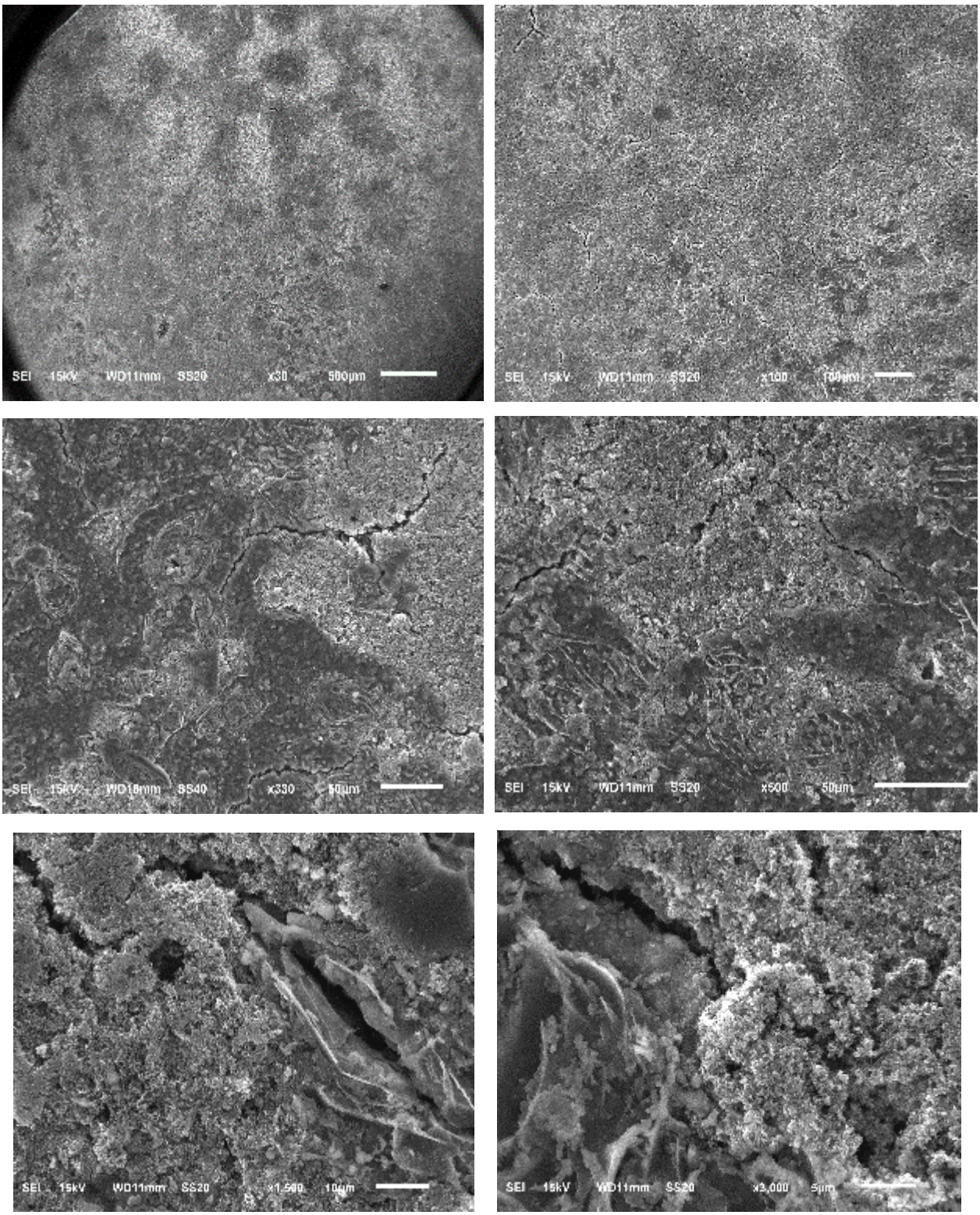

Figure S13. SEM images of $\mathbf{S_{cath}}$ cathode after 50 cycles.

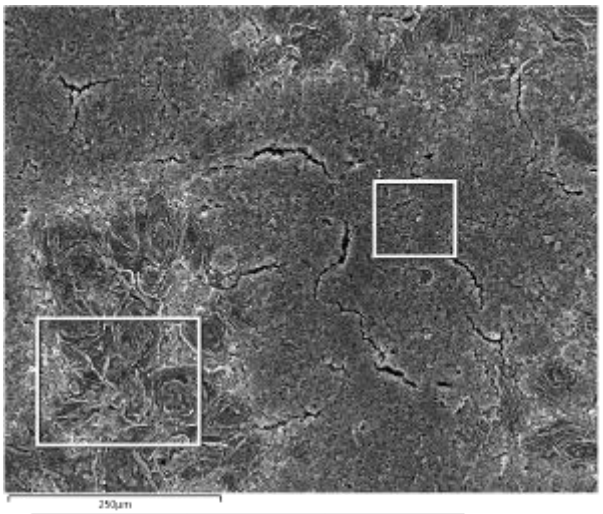

area	1	2
C	84.69	53.21
O	4.69	17.87
F	5.97	2.72
S	4.65	26.20
Total	100.00	100.00

area	1	2	3
C	40.94	39.03	77.50
O	24.20	24.35	6.49
F	2.30	1.89	5.86
S	32.57	34.73	10.15
Total	100.00	100.00	100.00

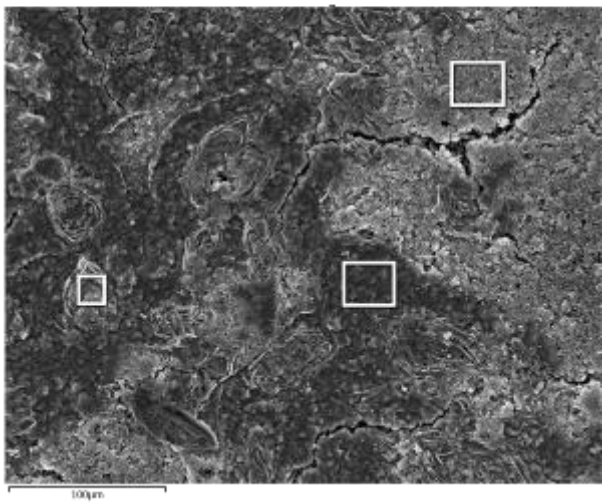

Figure S14. EDS analysis of selected regions on **S_{cath}** cathode after 50 cycles.

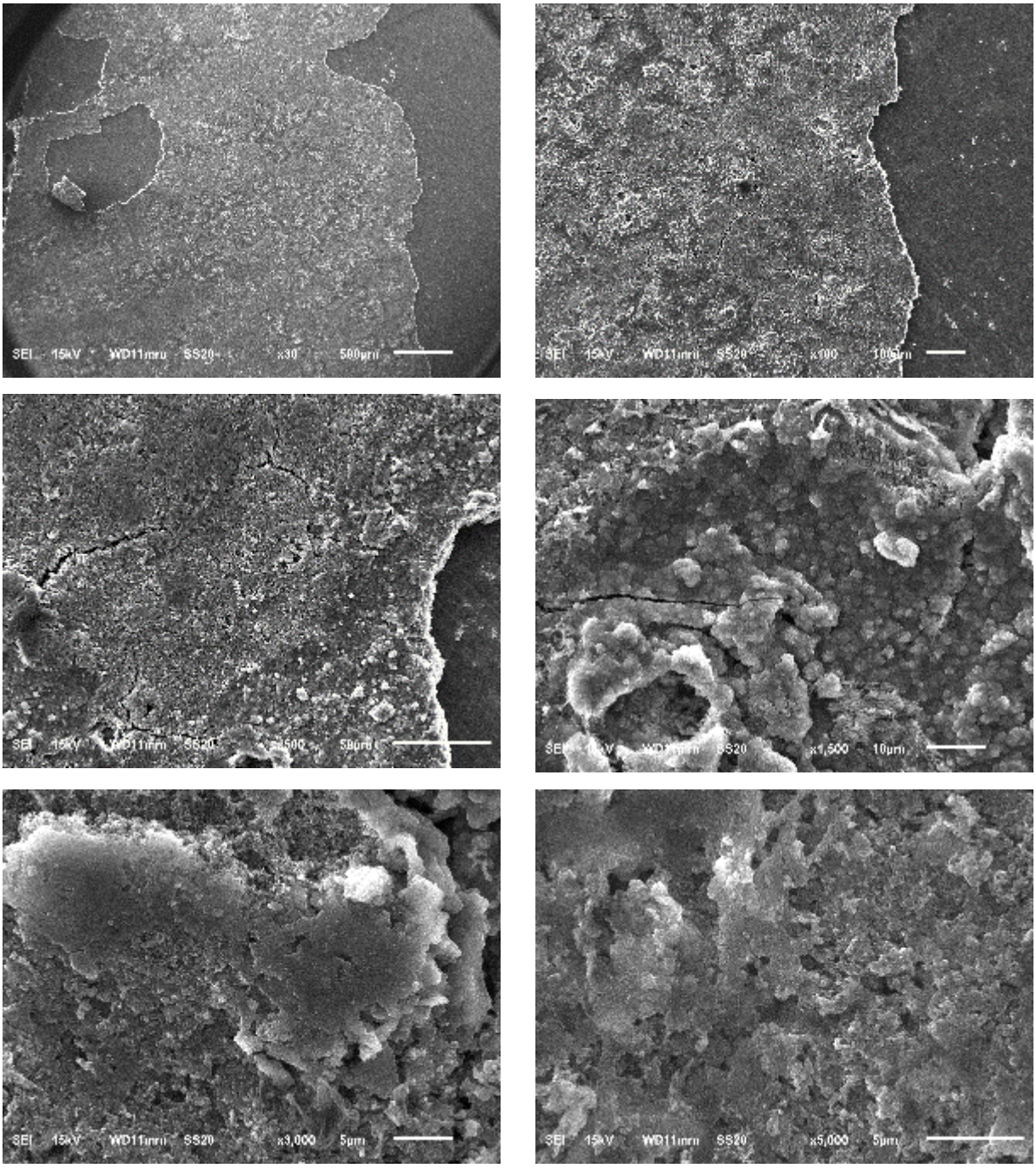

Figure S15. SEM images of **S-PAQ$_{cath}$** cathode after 50 cycles.

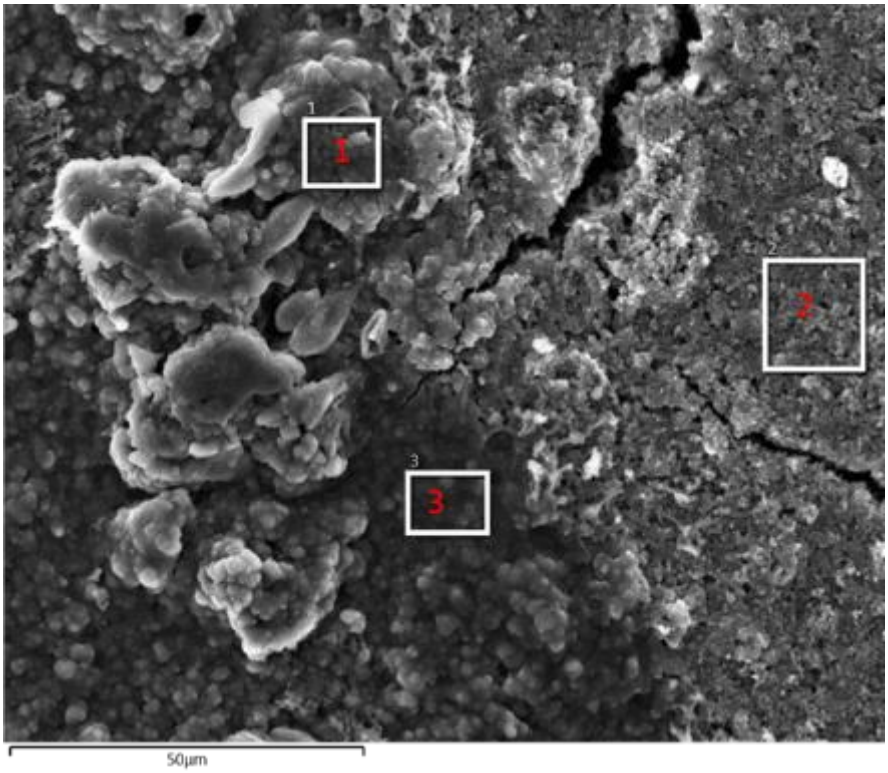

Area	1	2	3
C	43.55	68.78	40.17
O	14.80	9.67	15.48
F	3.77	5.04	4.91
Al	0.45	0.28	0.49
S	37.43	16.23	38.96
Total	100.00	100.00	100.00

Figure S16. EDS analysis of selected regions 1, 2, and 3 on **S-PAQ$_{cath}$** cathode after 50 cycles.

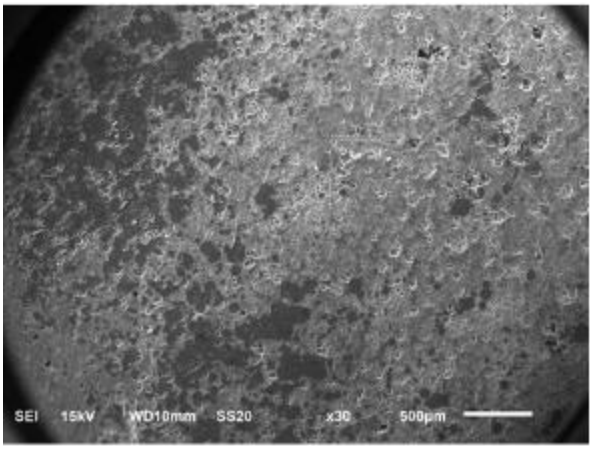

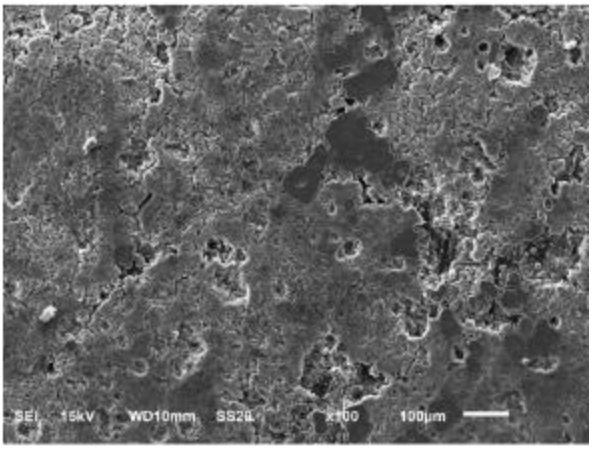

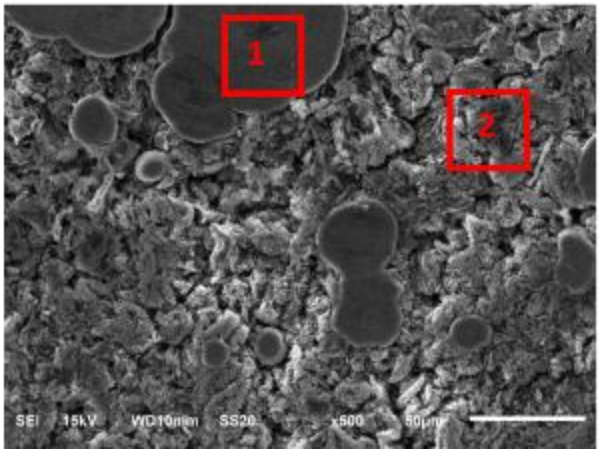

Area	1	2
C	35.65	37.18
O	3.51	21.34
F	2.77	0.98
S	58.06	40.49
Total	100.00	100.00

Figure S17. SEM images of Li anode and EDS analysis of selected regions on the anode for **S_{cath}** cell after 50 cycles.

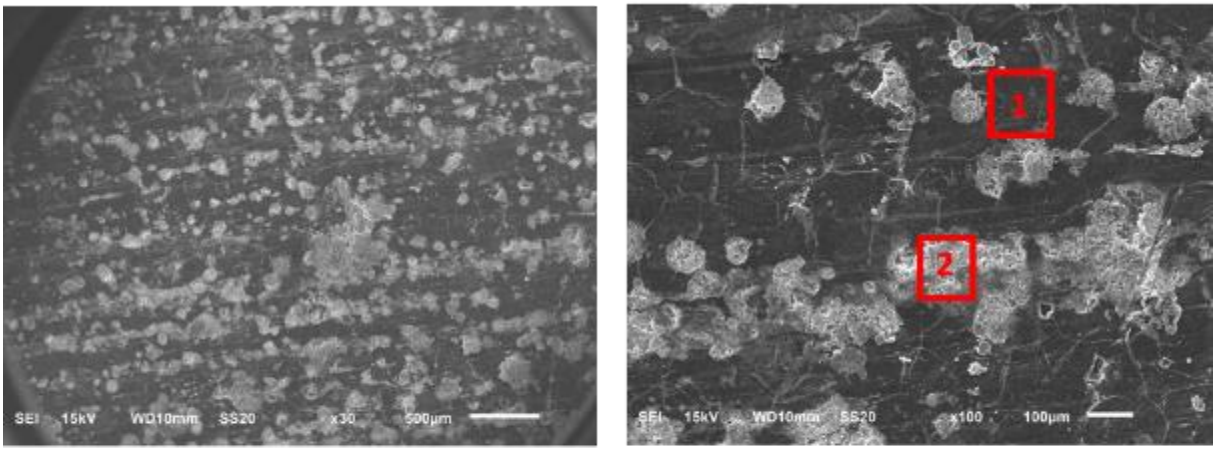

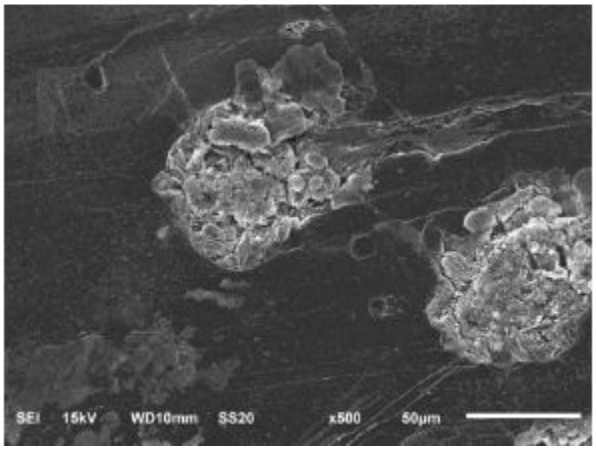

area	1	2
C	34.21	38.02
N	24.87	
O	39.54	23.03
F		
Al		0.77
S	1.38	38.17
Total	100.00	100.00

Figure S18. SEM images of Li anode and EDS analysis of selected regions 1 and 2 on the anode for **S-PAQ$_{cath}$** cell after 50 cycles.

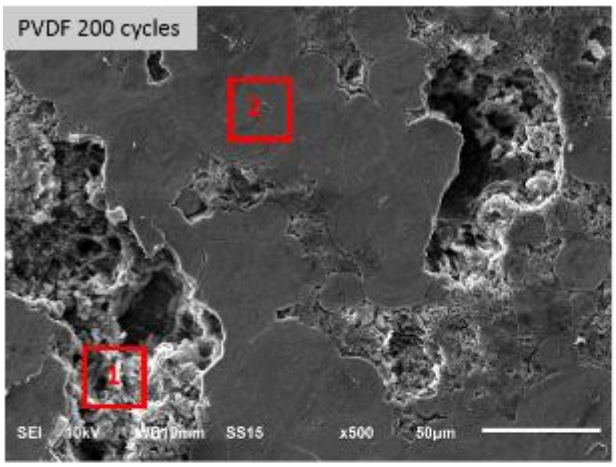

area	1	2
C	37.58	29.33
N	4.66	
O	15.45	3.43
F	1.81	3.31
S	40.51	63.94
Total	100.00	100.00

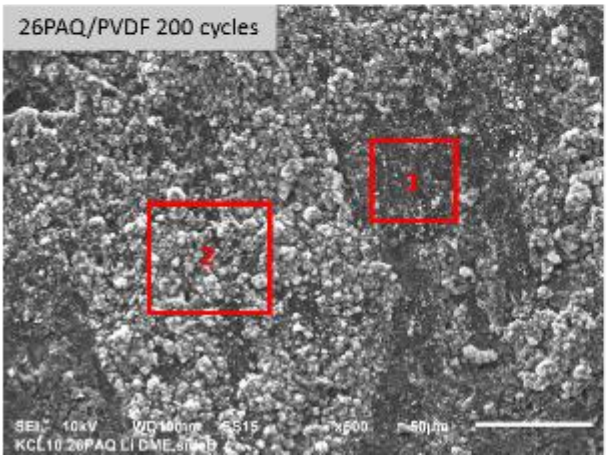

area	1	2
C	32.57	24.63
O	27.19	49.27
F	1.63	1.29
Al	0.93	0.33
S	37.67	24.48
Total	100.00	100.00

Figure S19. SEM images of Li anodes and EDS analysis of selected regions 1 and 2 on the anodes for **S_{cath}** (*top*) and **S-PAQ_{cath}** (*bottom*) cells after 200 cycles.

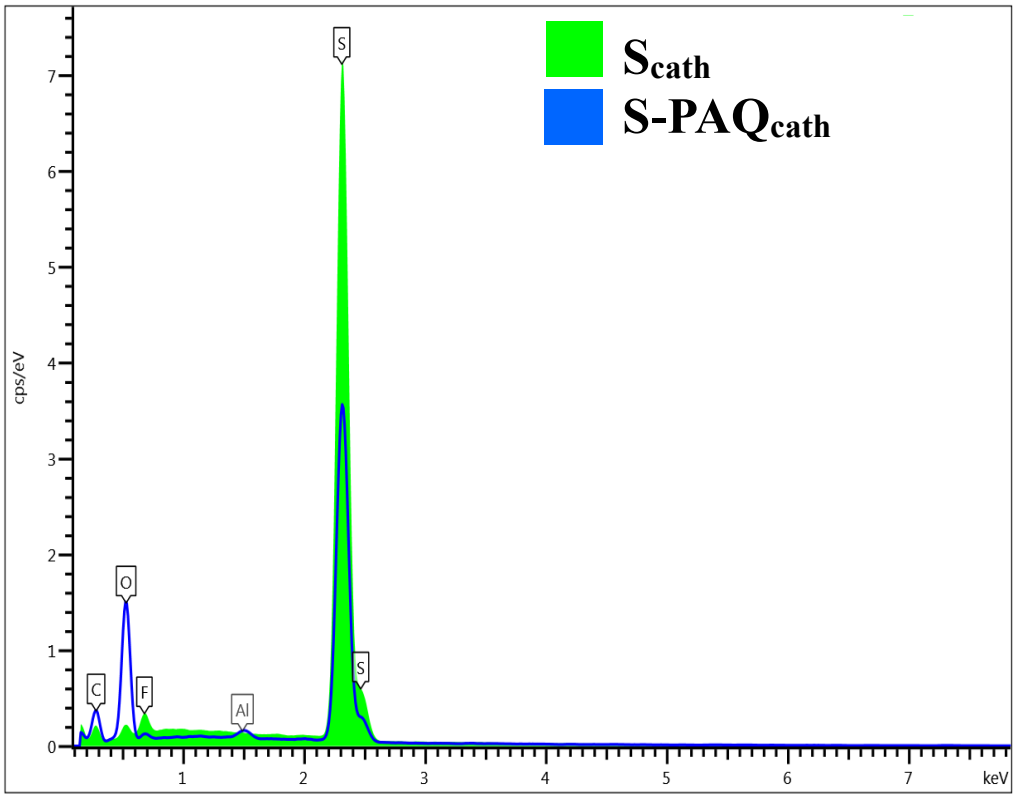

Figure S20. Comparison of EDS analyses for Li anodes in **S$_{cath}$** (*green*) and **S-PAQ$_{cath}$** (*blue*) cells after 200 cycles.

S7: Photographs of Li anodes

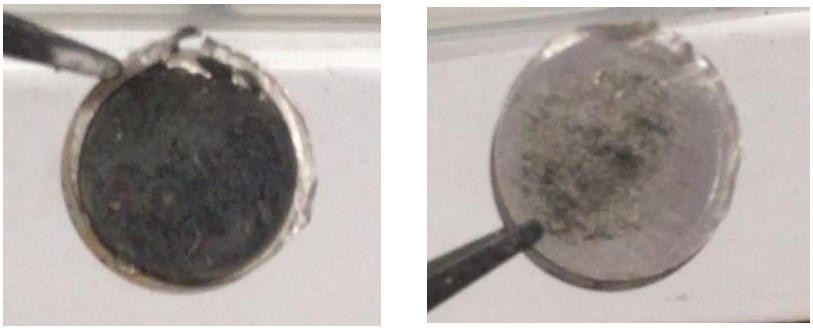

Figure S21. Photographs of Li anodes of **S_{cath}** (*left*) and **S-PAQ_{cath}** (*right*) cells showing the side of Li facing the separator.

S8. Supplementary X–ray photoelectron spectra

XPS survey spectra of Li anodes from the **S_{cath}** and **S-PAQ_{cath}** cells reveal the presence of S, O, C, N and F atoms on the surface (Figure S22), and quantification of their relative concentrations reveals a lower overall atomic fraction of S atoms on the Li anode from the **S-PAQ_{cath}** cell, which is consistent with the EDS analysis. Significantly, a higher degree of surface charging was observed during XPS measurements on Li from the **S_{cath}** cell, requiring charge compensation and resulting in broader linewidths (Figure 6, middle, main text). This strongly suggests the presence of a thicker layer of insulating Li_2S and Li_2S_n deposits, which is consistent with the significantly different appearance of the cycled Li electrodes (see main text and section S6-7). Semi-quantitative comparison of the deconvoluted F 1s core level spectra of these anodes suggests that LiF contributed to ~20 % of the signal and 2-3 at% total on the surface (Figure S23). Li 1s core level spectra show little LiF formation and shifting of peaks to higher binding energies presumably due to surface charging (Figure S24). C 1s core level spectra show overlapping signals from C-O, C=O, O=C-O species likely due to the decomposition of DME, which was used in washing Li, by Li (Figure S25). Very little signal corresponding to Li_2CO_3 and a CF_3 signal from LiTFSI were observed. The peak shape for the Li-Li symmetric cell may also be partially due to surface charging during measurement. O 1s core level spectra suggest a relatively higher fraction of Li_2O_2/Li_2O_x on the surface of the Li anode from the **S-PAQ_{cath}** cell, which is consistent with a higher oxygen atomic concentration on the Li anode from the **S-PAQ_{cath}** cell, in comparison with the **S_{cath}** cell (Figure S26). No peak at 528 eV was observed on any sample, indicating undetectable formation of Li_2O. An extra peak was present in the spectrum of the Li-Li symmetric cell, which strongly suggests surface charging. S 2p core level spectra reveals the deposition of Li_2S (160.6 eV) and Li_2S_n (161.7 eV) on Li metal, as well as a minor presence of elemental sulfur (163.4 eV; Table S3). SO_3^- signals resulting from the decomposition of LiTFSI (167.9 eV) and residual LiTFSI salt (169.6 eV) were also observed with both of these cells. The same XPS peaks were observed with a Li-Li symmetric cell that was cycled with the same electrolyte in the absence of S (Figure 6, main text). Overall, the presence of PAQ considerably reduces S deposition on Li.

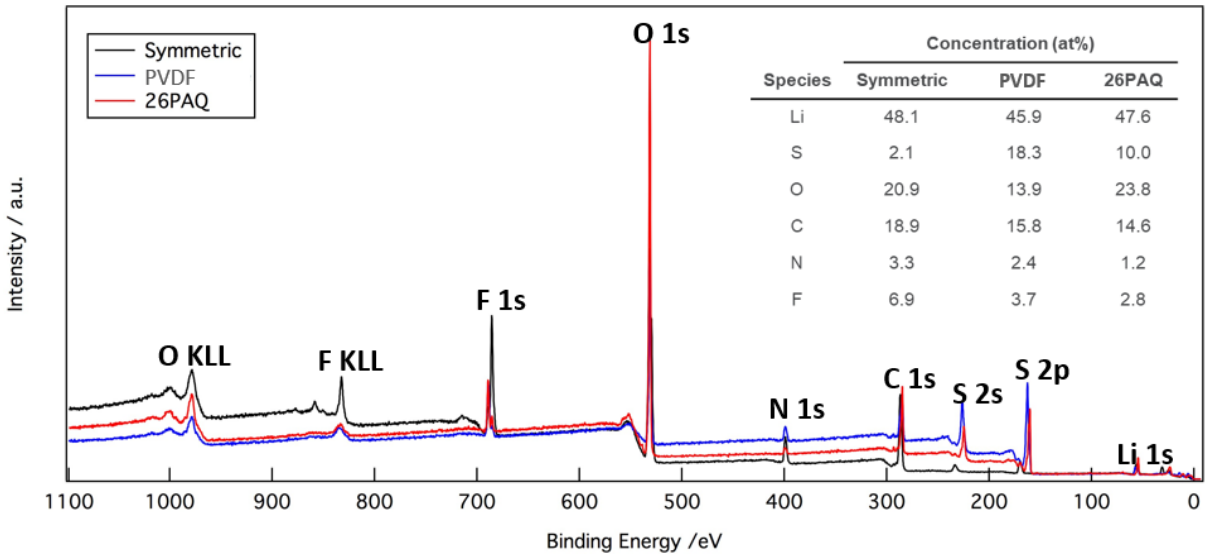

Species	Concentration (at%) Symmetric	PVDF	26PAQ
Li	48.1	45.9	47.6
S	2.1	18.3	10.0
O	20.9	13.9	23.8
C	18.9	15.8	14.6
N	3.3	2.4	1.2
F	6.9	3.7	2.8

Figure S22. Survey X-ray photoelectron spectra of Li anodes from Li-Li symmetric cell (*black*), **S$_{cath}$** cell (*blue*) and **S-PAQ$_{cath}$** cell (*red*).

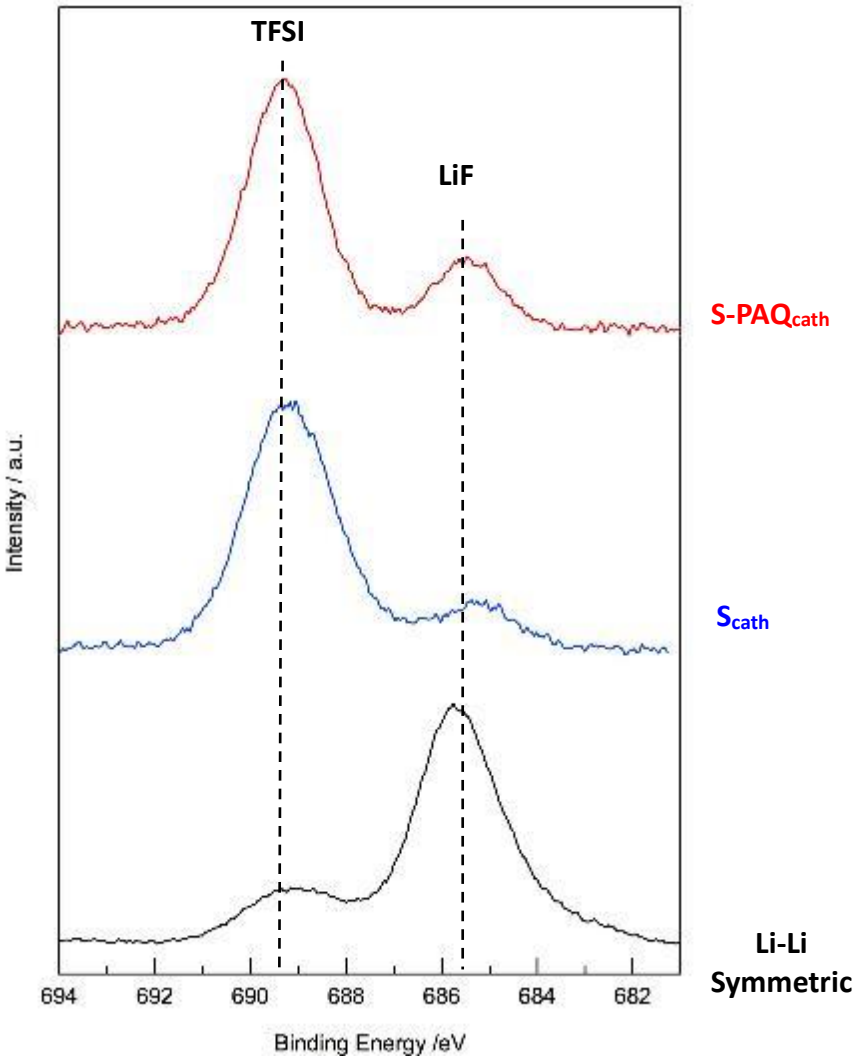

Figure S23. XPS F 1s spectra of Li anodes from **S-PAQ$_{cath}$** (*red*), **S$_{cath}$** (*blue*) and Li-Li symmetric (*black*) cells.

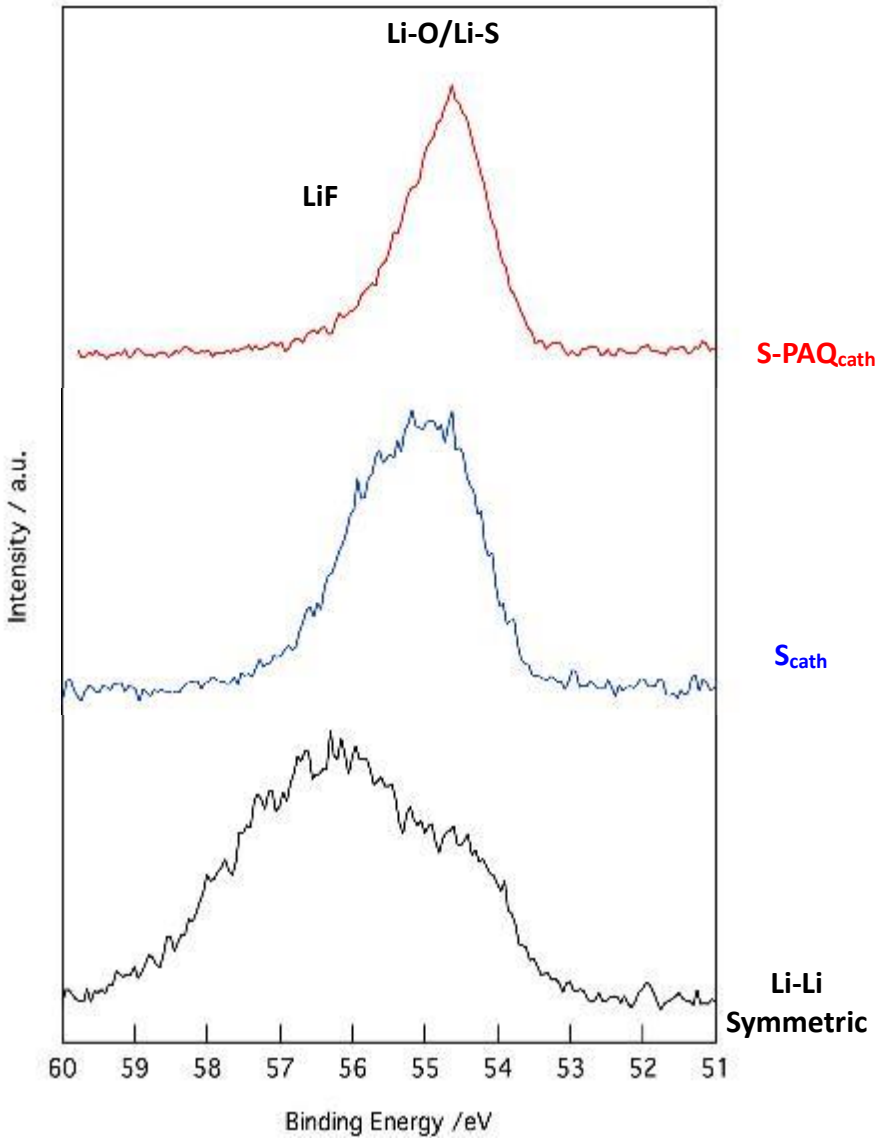

Figure S24. XPS Li 1s spectra of Li anodes from **S-PAQ$_{cath}$** (*red*), **S$_{cath}$** (*blue*) and Li-Li symmetric (*black*) cells.

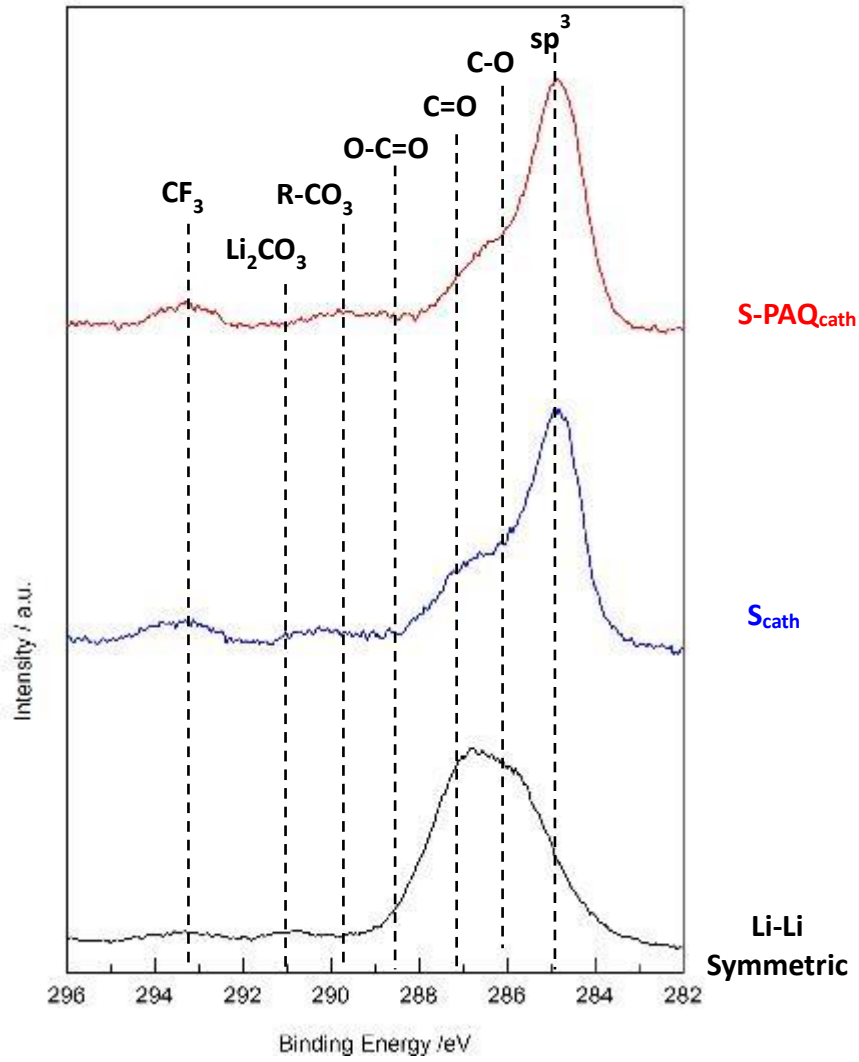

Figure S25. XPS C 1s spectra of Li anodes from **S-PAQ$_{cath}$** (*red*), **S$_{cath}$** (*blue*) and Li-Li symmetric (*black*) cells with the partial band attributions.

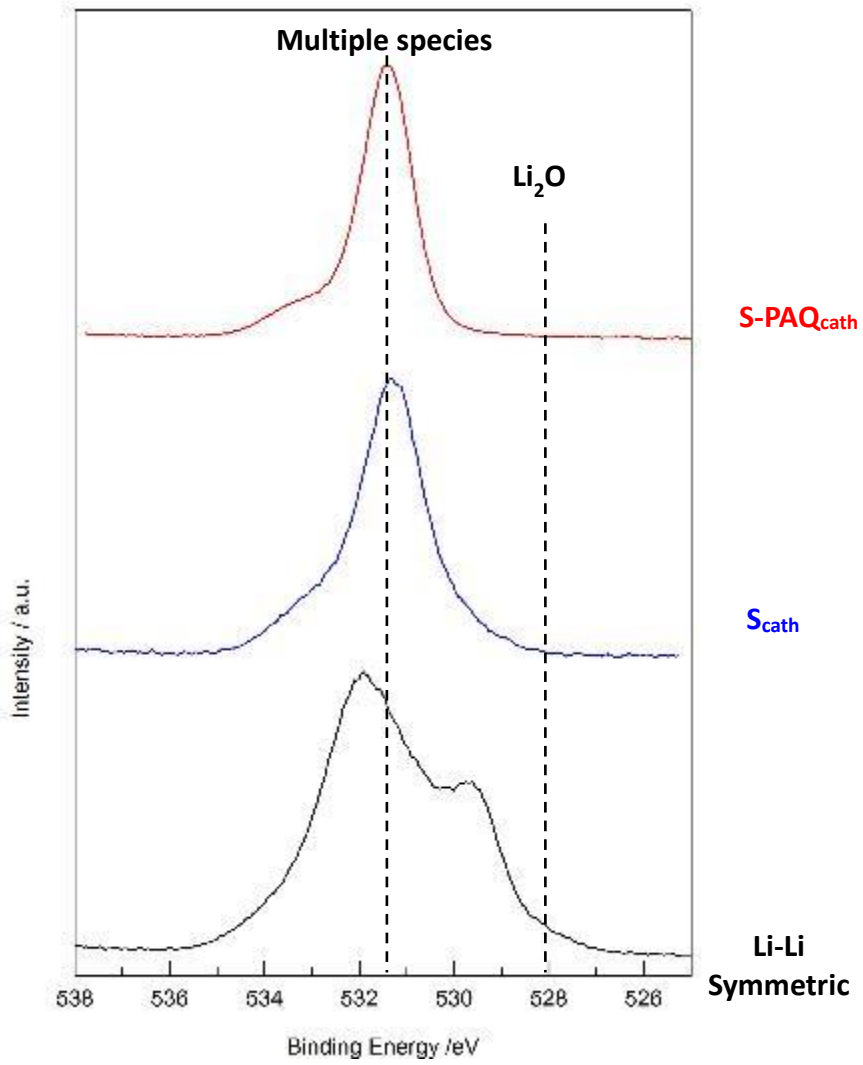

Figure S26. XPS O 1s spectra of Li anodes from **S-PAQ$_{cath}$** (*red*), **S$_{cath}$** (*blue*) and Li-Li symmetric (*black*) cells.

Table S3. Relative contents of various sulfur species observed in S 2p core level X-ray photoelectron spectra

	Relative Concentration (at%)		
Sulfur Species	**S-PAQ$_{cath}$**	**S$_{cath}$**	**Li-Li Symmetric**
S^{2-}	64.5	65.3	1.2
S^{-}	15.4	13.3	1.8
S^{0}	9.8	13.5	2.3
SO_3^{-}	2.9	1.0	32.3
TFSI/SO_4^{2-}	7.4	6.9	62.3

S9. NMR and thermogravimetric analyses (TGA).

To quantify the presence of the solvent in the Li[PAQ] material for magnetic measurement in section S2, two methods were used. With the first method, the dry powder was weighted and suspended in CD_3CN that contained ferrocene as an internal standard. The proton NMR spectrum was obtained, and the resonance lines from the residual THF and pentane were integrated and compared to the ferrocene resonance. In this way, we determined that the polymer sample contained 9.3 wt% THF (which corresponds to 3 THF molecule per 10 units) and 1.6 wt% pentane. For additional control, thermogravimetry analysis (TGA) was carried out using a Perkin Elmer Pyris 1TGA analyzer. We thank Javier Bareño of CSE/ANL for helping us with this analysis. The loaded sample (3.216 mg) was held at 30 ºC for 5 min, and then the temperature was ramped to 350 ºC at 5 ºC/min. The resulting mass loss is shown in Figure S27. During the initial stage, ≈ 0.6 wt% of the sample was lost, and in the second stage (the second linear section in the plot) *ca.* 10.3 wt% mass was lost at 120 ºC. The subsequent warming to 350 ºC resulted in the gross loss of 19 wt%. We believe that this high-temperature mass loss was due to thermolysis of the polymer sample, whereas the mass loss below 120 ºC corresponded to the removal of the residual solvent. Our TGA estimate for the added mass of the solvent (10.3 wt%) is in excellent agreement with our ^{1}H NMR estimate (10.9 wt%).

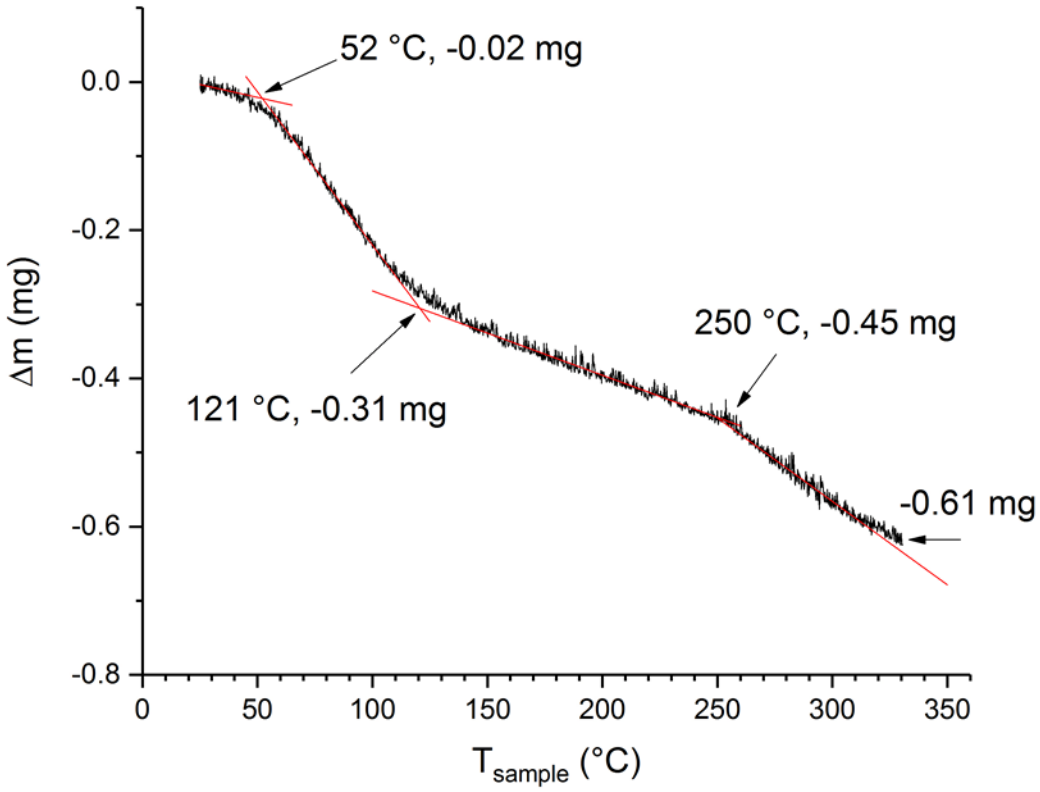

Figure S27. Mass loss in the Li[PAQ] sample (with the initial mass of 3.216 mg) during the programmed warming of this sample from 25 °C to 350 °C.

S10. Additional references

1. Zhou, Y.; Wang, B.; Liu, C.; Han, N.; Xu, X.; Zhao, F.; Fan, J.; Li, Y. *Nano Energy* **2015**, *15*, 654.
2. Pan, B.; Huang, J.; Feng, Z.; Zeng, L.; He, M.; Zhang, L.; Vaughey, J. T.; Bedzyk, M. J.; Fenter, P.; Zhang, Z.; Burrell, A. K.; Liao, C. *Adv. Energy Mater.* **2016**, *6*, 1600140.
3. Lukasiewicz, M.; Bogdal, D.; Pielichowski, J. *Adv. Synth. Catal.* **2003**, *345*, 1269.
4. Amicangelo, J. C.; Leenstra, W. R. *Inorg. Chem.* **2005**, *44*, 2067.
5. Yang, J.; Dass, A.; Rawashdeh, A.-M. M.; Sotirious-Leventis, C.; Panzner, M. J.; Tyson, D. S.; Kinder, J. D.; Leventis, N. *Chem. Mater.* **2004**, *16*, 3457.
6. Gladysz, J. A.; Wong, V. K.; Jick, B. S. *J. Chem. Soc., Chem. Commun.* **1978**, *19*, 838.
7. Hatfield, W. E. *J. Appl. Phys.* **1981**, *52*, 1985.
8. Chen. K. S. *Proc. Natl. Sci. Counc. (Taiwan) Part 1*, **1977**, *10*, 195.